View metadata, citation and similar papers at core.ac.uk

brought to you by CORE

provided by Archivio istituzionale della ricerca - Università di Trieste

Journal of South American Earth Sciences xxx (2016) xxx-xxx

Contents lists available at ScienceDirect

Journal of South American Earth Sciences

journal homepage: www.elsevier.com

Late-stage magmatic to deuteric/metasomatic accessory minerals from the Cerro Boggiani agpaitic complex (Alto Paraguay Alkaline Province)

Piero Comin-Chiaramonti [a, **], Alberto Renzulli [b, *], Filippo Ridolfi [b], Gaston E.R. Enrich [c], Celso B. Gomes [c], Angelo De Min [a], Rogério G. Azzone [c], Excelso Ruberti [c]

[a] *Dipartimento di Matematica e Geoscienze, University of Trieste, Via Weiss 8, I-34127 Trieste, Italy*
[b] *Dipartimento di Scienze Pure e Applicate, University of Urbino, Campus Scientifico "Enrico Mattei", Via Cà Le Suore 2-4, 61029 Urbino, Italy*
[c] *Instituto de Geociências, University of São Paulo, Cidade Universitária, Rua do Lago 562, 05508-080 São Paulo, Brazil*

ARTICLE INFO

Article history:
Received 24 March 2016
Received in revised form 22 July 2016
Accepted 8 August 2016
Available online xxx

Keywords:
REE-bearing minerals
Carbonates
Zirconosilicates
Peralkaline
Agpaitic
Deuteric
Metasomatic
Carbonatitic fluids
Cerro Boggiani
Paraguay

ABSTRACT

This work describes rare accessory minerals in volcanic and subvolcanic silica-undersaturated peralkaline and agpaitic rocks from the Permo-Triassic Cerro Boggiani complex (Eastern Paraguay) in the Alto Paraguay Alkaline Province. These accessory phases consist of various minerals including Th—U oxides/silicates, Nb-oxide, REE-Sr-Ba bearing carbonates-fluorcarbonates-phosphates-silicates and Zr—Na rich silicates. They form a late-stage magmatic to deuteric/metasomatic assemblage in agpaitic nepheline syenites and phonolite dykes/lava flows made of sodalite, analcime, albite, fluorite, calcite, ilmenite-pyrophanite, titanite and zircon. It is inferred that carbonatitic fluids rich in F, Na and REE percolated into the subvolcanic system and metasomatically interacted with the Cerro Boggiani peralkaline and agpaitic silicate melts at the thermal boundary layers of the magma chamber, during and shortly after their late-stage magmatic crystallization and hydrothermal deuteric alteration.

© 2016 Published by Elsevier Ltd.

1. Introduction

Accessory minerals of the silica-undersaturated peralkaline Cerro Boggiani complex, at the border of Brazil and Paraguay have been studied in detail within the framework of a collaborative scientific program involving researchers from Brazil and Italy.

The rock types are agpaitic nepheline syenites and phonolites composed of alkali feldspar (52–60 vol%), nepheline (15–28 vol%), locally abundant sodalite (8–17 vol%), sodic clinopyroxene (4–16 vol%), scarce biotite (annite-rich: 0.2–0.5 vol%) and amphibole (katophorite-richterite: 0.2–0.9 vol%; cf. Tab. 34 of Comin-Chiaramonti et al., 2005) with primary accessories (titanite, magnetite, ilmenite, zircon and aenigmatite), and a wide range of very late-crystallized phases which are often difficult to analyse quantitatively owing to their small size or their volatile nature under the electron beam. Minerals identified so far include ancylite, bastnäsite-parisite-synchysite, britholite, burbankite, cordylite, eudialyte (subordinately Ca-catapleiite), låvenite, pyrochlore, rosenbuschite, thorite and uraninite-thorianite, usually related to late-stage magmatic crystallization, deuteric and/or metasomatic fluids (Castorina et al., 1997; Enrich et al., 2010, 2011, 2012) enriched in rare earth elements, fluorine, chlorine, H_2O and CO_2.

This paper reports the composition and textural relationships of these accessory minerals (see also Comin-Chiaramonti et al., 2005, Carbonin et al., 2005; Enrich et al., 2010, 2011, 2012), which are generally very similar to those found in other peralkaline rocks worldwide (e.g. Junguni intrusion, Malawi, after Woolley and Platt, 1988; Agua de Pau Volcano, Azores, after Ridolfi et al., 2003; Kilombe Volcano, Kenia, after Ridolfi et al., 2006). A sequence of crystallization of the investigated accessory minerals is also emphasized.

2. Geological background

In the Alto Paraguay Province (APP), alkaline magmatism occurs along the Paraguay River (Fig. 1). It consists of a series of stocks and ring complexes cropping out along both riverbanks, mainly to the north and south of Porto Murtinho city in the Mato Grosso do Sul State, Brazil. Radiometric ages of this magmatic activity have recently been reviewed by Comin-Chiaramonti et al. (2015 and references therein). The average K/Ar and Ar/Ar ages were determined as 248.8 ± 4.8 Ma and 241.8 ± 1.1 Ma, while best values of Rb/Sr and Sm/Nd isochrons point to ages of 244 ± 27 Ma and 256 ± 3 to 257 ± 3 Ma, respectively. These ages show that the complexes were

* Corresponding author.
** Corresponding author.
Email address: alberto.renzulli@uniurb.it (A. Renzulli)

http://dx.doi.org/10.1016/j.jsames.2016.08.003
0895-9811/© 2016 Published by Elsevier Ltd.

UNCORRECTED PROOF

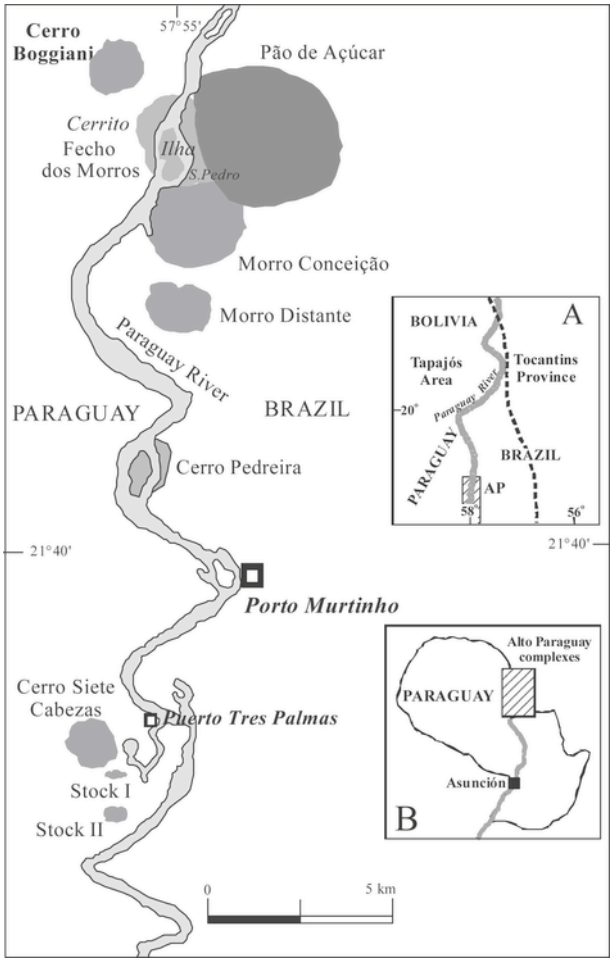

Fig. 1. Sketch map showing the main alkaline igneous rock occurrences of the Alto Paraguay Alkaline Province (Comin Chiaramonti et al., 2005 and references therein). Inset A: Map representing the Tocantíns Neoproterozoic orogenic area (Madeiro subprovince, after Amaral, 1984; Soares et al., 2006) and the adjacent Paleoproterozoic Tapajos Province (Lemarão et al., 2002) separated by a bold, dotted line. AP: Alto Paraguay alkaline complexes. Inset B: position of the Alto Paraguay alkaline complexes within Paraguay.

emplaced during the Early Triassic and represent the oldest magmatic activity around the Paraná Basin, tectonically related to the Tapajós and Tocantins Provinces, after the Brasiliano cycle (Comin-Chiaramonti et al., 2015 and references therein).

APP consists of seven major circular complexes (from north to south: Cerro Boggiani, Pão de Açúcar, Fecho dos Morros, Morro Conceição, Morro Distante, Cerro Pedreira and Cerro Siete Cabezas) and some minor stocks, lava flows and dykes (Fig. 1). Intrusive to subvolcanic rocks are mostly sodic in composition and mainly represented by nepheline syenites, syenites, quartz-bearing syenites and their corresponding extrusive rock types (i.e. phonolites and trachytes). Miaskitic (slightly agpaitic, with rare minerals having alkalinity modulus, K_{alk}, ≪15 as defined by Khomyakov, 1995) and agpaitic (with rare minerals with K_{alk} = 15–40) suites characterize the southern (Cerro Siete Cabezas) and northern (Cerro Boggiani, Pão de Açúcar, Fecho dos Morros-Cerrito) occurrences, respectively (Comin-Chiaramonti et al., 2014). It is worth to note the term agpaitic should be restricted to peralkaline nepheline syenites and phonolites containing complex silicate minerals of Zr, Ti, REEs, fluorine and other volatiles (such as eudialyte, Sørensen, 1997). In this way, the Cerro Boggiani nepheline normative rocks having a peralkaline index (also referred to as agpaitic index, A.I.) between 1.1 and 1.5 (Gomes et al., 1996; cf. Tab. 35 of Comin-Chiaramonti et al., 2005) and also containing the above complex silicate minerals (with K_{alk} 15–40), can be considered agpaitic *stricto sensu*. Cerro Boggiani consists of a small hill, 0.5 km in diameter and <140 m high, associated with two satellite plugs and dykes cropping out above the alluvial sediments of the Paraguay river (Putzer and Van den Bomm, 1962). Overall, the intrusions seem to define a circular structure extending over 4 km^2 (Comin-Chiaramonti et al., 2005).

3. Petrography and chemical features

Cerro Boggiani intrusive complex (21°24′00″S and 57°56′50″) is located ca. 2.5 km NW of the Pão de Açúcar volcanic centre (Fig. 1) and consists mainly of foid syenites and nepheline syenites with modal nepheline and sodalite contents of 16–28 and 8–17 vol%, respectively. The lithotypes are medium to coarse-grained and allotriomorphic in texture, and contain abundant perthitic alkali feldspar (up to 60 vol%). They also have clinopyroxene (aegirine-augite to aegirine, up to 8 vol%) as the most abundant mafic phase, and amphibole (ferrorichterite to arfvedsonite, 0.2–0.9 vol%) partially replacing the former at the rims (±biotite) and accessory phases such as ilmenite-pyrophanite, titanite and apatite. In addition, late-stage magmatic to deuteric/metasomatic accessory minerals, such as aenigmatite, ancylite, bastnäsite-parisite-synchysite, britholite, burbankite, Ca-catapleiite, eudialyte, låvenite, pyrochlore, rosenbuschite, thorite, uraninite-thorianite and carbonates, occur locally. Carbonates, cancrinite and zeolites usually point out the post-magmatic conditions of crystallization (Fig. 2).

On the other hand, extrusive rocks (lava flows and dikes) cluster in the phonolite field (Fig. 3A). They are characterized by an aphanitic groundmass with phenocryst and/or microphenocryst of alkali feldspar, nepheline (up to 20 vol%), sodalite and subordinate aegirine-augite, sodic amphibole, aenigmatite and biotite set in a very fine trachytoidal matrix. Main accessory phases are apatite, eudialyte, låvenite, pyrophanite, rosenbuschite, titanite and uraninite; carbonates can be also present as patches and/or veins (Comin-Chiaramonti et al., 2005). Deuteric and metasomatic conditions of crystallization (Stoppa and Schiazza, 2014) are emphasized by the presence of cancrinite and zeolites.

The primary mineralogical assemblages indicate emplacement temperatures of 700–1000 °C and, for intrusive rock-types, a very low total pressure, i.e. around 1 kb, with high fluorine activity. By contrast, the association of aenigmatite, ilmenite and annite-rich biotite suggests subsolidus reactions developing at the intersection of Ac-Ilm-Aen buffer with the Na-amphibole and annite stability field (cf. Nicholls and Carmichael, 1969) at temperatures around 500–570 °C (cf. Comin-Chiaramonti et al., 2005).

An Agpaitic (Peralkaline) Index (A.I.) vs. Quartz/Nepheline (Q-Ne) normative diagram (Fig. 3) shows that both intrusive and extrusive rocks from Cerro Boggiani have a strong peralkaline character, with A.I. as high as 1.5 (cf. Table 35 of Comin-Chiaramonti et al., 2005). Modal content of accessory phases averages 2.6 ± 0.9 vol%. Compositions of four representative samples, three phonolites (RP28, RP31A, RP41) and one nepheline syenite (RP38B), are reported in Table 1. Whole-rock spider diagrams of incompatible elements (Fig. 4) show positive anomalies of U—Th, Nb—Ta, La-Ce-Nd and Zr—Hf, which are related to both the alkaline affinity and the mineral chemistry of late-stage magmatic to deuteric and/or metasomatic accessory phases.

The isotopic C—O values (δ‰) in calcite of additional samples are reported in Table 2. It should be noted that these samples contain

UNCORRECTED PROOF

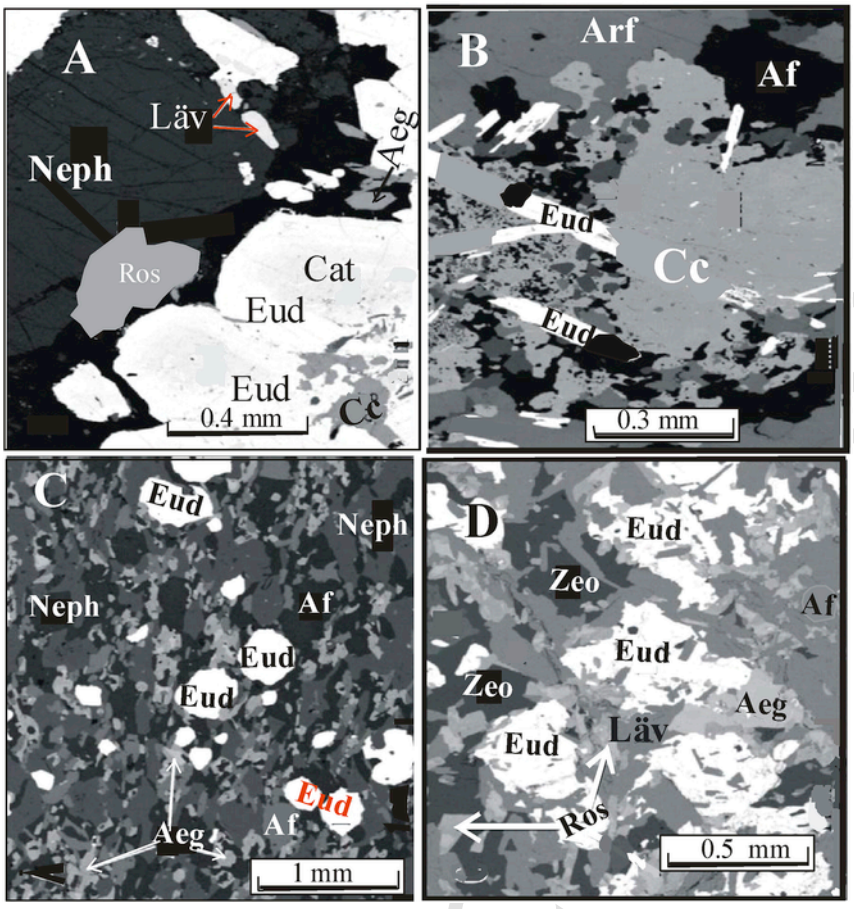

Fig. 2. Back-scattered Scanning Electron Microscope (SEM) images of fundamental and accessory minerals from the Cerro Boggiani agpaitic alkaline igneous rocks. **A**: large eudialyte (Eud) from nepheline syenite (RP33B) with catapleiite (Cat), nepheline (Neph), calcite (Cc), rosenbuschite (Ros) and låvenite (Låv); **B**: nepheline syenite (RP33B) showing eudialyte (Eud), arfvedsonite (Arf), calcite (Cc) and alkali feldspar (Af); **C**: fine grained eudialyte (Eud) in phonolitic lava flow (RP31A) associated with nepheline (Neph), alkali feldspar (Af) and aegirine (Aeg); **D**: eudialyte in nepheline syenite (RP33B), with zeolites (Zeo), aegirine (Aeg), alkali feldspar (Af) and rosenbuschite (Ros).

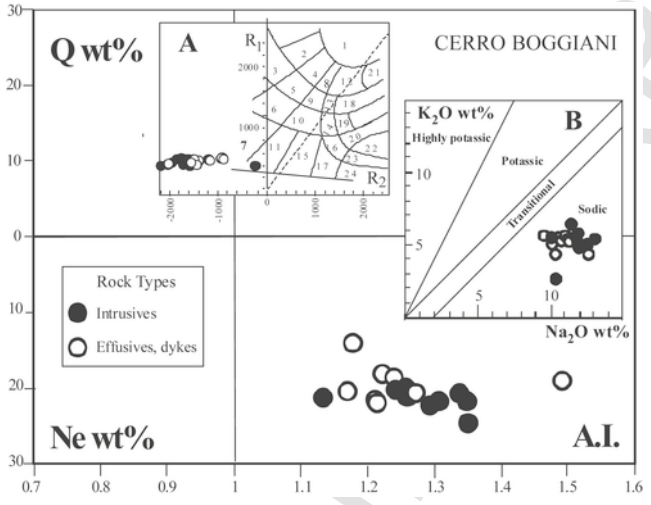

Fig. 3. Cerro Boggiani complex (data from Comin-Chiaramonti et al., 2005): agpaitic index [A.I. = $(Na_2O + K_2O)/Al_2O_3$, molar ratio] vs. normative quartz (Q) and nepheline (Ne) for sodic rock-types. Inset **A**: R_1-R_2 classification diagram according to De La Roche et al. (1980) showing field7, i.e. nepheline syenite-phonolite. Inset **B**: Na_2O vs. K_2O wt% diagram (after Le Maitre, 1989) displaying the sodic field occupied by the Cerro Boggiani samples.

0.46–0.96 wt% of CO_2, corresponding to $CaCO_3$ equivalent contents of 1.00–2.18 wt%. Table 2 shows that the average CO_2/H_2O ratio is 0.84 ± 0.03. Notably, this ratio and the isotopic C—O values are representative of a hydrothermal environment (Fig. 5), as also indicated by curve I of the Cerro Chiriguelo wells (cf. also Fig. 8 of Comin-Chiaramonti et al., 2014).

The following paragraphs will describe the rare accessory minerals of Cerro Boggiani, roughly corresponding to the positive anomalies in the whole-rock incompatible elements, i.e. thorianite-uraninite-thorite (U, Th), pyrochlore (Nb), REE minerals, rosenbuschite, låvenite, eudialyte (Zr—Hf).

4. Analytical methods

Modal mineralogy and mineral chemistry of the main phases (i.e. clinopyroxene, amphibole, aenigmatite, biotite, mesoperthite, sodic sanidine, nepheline, sodalite and ilmenite) from the Cerro Boggiani alkaline complexes are described in Comin-Chiaramonti et al. (2005). Accordingly, only the rare accessory phases are discussed here.

Quantitative analyses were performed on carbon-coated thin sections by wavelength dispersion method (WDS) at Padova (Italy) and São Paulo (Brazil) universities. In Padova (Institute of Geosciences and Georesources, CNR), the analyses were performed using a Cameca/Camebax electron microprobe with accelerating voltage and beam current ranging between 15 and 20 kV and 10–20 nÅ, respec-

Table 1
Representative whole-rock compositions of the Cerro Boggiani alkaline complex (major and trace elements are from Tables 35 and 40 of Comin-Chiaramonti et al., 2005). REE, Th, U, Hf and Ta were analysed by ICP-MS –Perkin Elmer Elan 5000 in a solution obtained by mixed HF—$HClO_4$ digestion in sealed and pressurized Teflon vessels, following procedures outlined by Alaimo and Censi (1992). R1 and R2 classification following De La Roche et al., 1980; A.I., agpaitic index ($Na_2O + K_2O/Al_2O_3$ molar ratio).

Major elements	RP28 dyke	RP31A lava flow	RP38B intrusive rock	RP41 lava flow
Major elements (wt%)	Phonolite	Phonolite	Nepheline syenite	Phonolite
SiO_2	57.83	57.46	57.57	57.01
TiO_2	0.35	0.51	0.18	0.23
Al_2O_3	19.42	18.86	19.07	18.90
FeOtot	2.33	3.14	4.60	4.68
MnO	0.14	0.22	0.21	0.25
MgO	0.10	0.26	0.05	0.07
CaO	0.96	1.33	1.18	1.06
Na_2O	11.98	11.41	10.15	10.82
K_2O	5.83	5.46	5.59	5.55
P_2O_5	0.02	0.14	0.09	0.01
H_2O^+	0.55	0.92	1.10	0.88
CO_2	0.46	0.81	0.96	0.73
Sum	99.97	100.52	100.75	100.19
R_1	−1838	−1600	−1276	−1478
R_2	489	524	502	488
A.I.	1.34	1.31	1.19	1.26
Trace elements (ppm)				
Ba	100	437	135	13
Rb	247	243	291	354
U	12.1	17.01	14.3	1.80
Th	3.9	11.53	10.1	5.6
Nb	149	237	128	186
Ta	19.4	16.09	16.62	17.0
La	139	137	96	54.0
Ce	204	225	143	71.9
Sr	133	319	104	72
Nd	46	59	33	11.3
Sm	5.81	6.79	4.75	1.5
Zr	1696	1499	1670	2239
Hf	33.10	33.75	34.73	70.3
Tb	0.97	1.03	0.67	0.30
Y	34	55	33	23.3
Tm	0.85	1.16	0.70	0.50
Yb	5.76	5.72	4.70	4.30

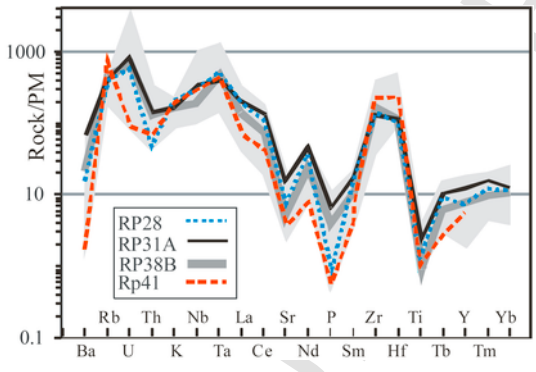

Fig. 4. Spider diagrams (PM, according to Sun and McDonough, 1989) for representative samples of Cerro Boggiani (RP28, phonolite dyke; RP31A, phonolite lava flow; RP38B, nepheline syenite; RP41, phonolite lava flow) normalized to primitive mantle. Grey field represents the general variation for all the Cerro Boggiani samples (cf. data of Tables 35 and 40, and Fig. 43 of Comin-Chiaramonti et al., 2005).

Table 2
Measured isotope compositions of carbonate fractions of alkaline rocks at Cerro Boggiani. C—O isotopic values (δ‰) were determined on the carbonate fractions according to Censi et al. (1989): the oxygen and carbon data of carbonate fractions from selected whole rocks were obtained by reacting the samples with 100% H_3PO_4 at 25 °C. The CO_2 released was subsequently analysed in a Finnigan Mat Delta S mass spectrometer and its oxygen isotopic composition corrected to calcite by a fractionation factor of 1.01025 (cf. Speziale et al., 1997 and references therein). The powder sample prepared with grain size ranging between 100 and 200 mesh and the CO_2 corresponding to calcite was extracted 1 h after reaction. The isotopic results are given in terms of usual δ‰, the reference standards being PDB-1 and V-SMOW for carbon and oxygen isotopes, respectively.

Sample	RP27	RP28	RP31A	RP33	RP38B	RP41
H_2O	0.94	0.55	0.92	0.54	1.10	0.88
CO_2	0.78	0.46	0.81	0.44	0.96	0.73
CO_2/H_2O	0.83	0.84	0.88	0.81	0.88	0.83
$CaCO_3$ equivalent	1.77	1.05	1.84	1.00	2.18	1.66
$\delta^{13}C$ (PDB-1)‰	+0.1	−1.8	−2.5	−4.0	−1.3	−0.5
$\delta^{18}O$ (V-SMOW)‰	+17.8	+14.5	+14.0	+11.9	+15.6	+17.1

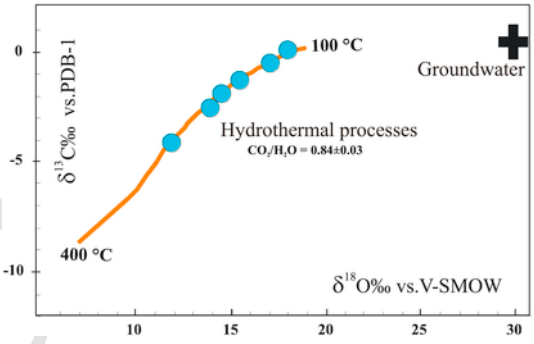

Fig. 5. Plot of $\delta^{18}O$ vs. $\delta^{13}C$ for carbonates from Cerro Boggiani (cf. Table 2) and evolution of the oxygen-carbon isotope composition in a hydrothermal environment, i.e. 400–100 °C, according to Castorina et al. (1997) and Comin-Chiaramonti et al. (2005). Arbitrary composition of groundwater: $\delta^{18}O = 30‰$, $\delta^{13}C = 0$ (after Taylor, 1978 and Usdowski, 1982).

tively (depending on the phase stability). X-ray counts were converted into oxide mass percentages by a PAP correction program provided by Cameca Minerals (Carbonin et al., 2005). In São Paulo (Instituto de Geociências), the analytical work was performed employing a Jeol JXA 8600 electron microprobe equipped with a Voyager Noran automation system. Analytical conditions for BSE imaging, quantitative WDS and qualitative EDS analyses were 15 kV for accelerating voltage and 20 nÅ for electron beam current. The data were processed utilizing the PROZA procedure (Bastin et al., 1984). In both laboratories, special care was taken in selecting peak and background positions in order to eliminate peak overlapping. Peak counting times were 10–20 s for F, Na, Mg, Al, Si, P, Cl, S, K, Ca, Fe, Mn, and Ti, and 60 s for the other elements. Natural minerals and synthetic materials were used as standards: $ThSiO_4$ (Si$K\alpha$), TiO_2 (Ti$K\alpha$), zircon (Zr$L\alpha$), $HfSiO_4$ (Hf$L\alpha$), Nb (Nb$L\alpha$), Ta (Ta$L\alpha$), plagioclase An_{50} (Al$K\alpha$), Y-garnet (Y$L\alpha$), synthetic Ca—Al-silicate glasses (La$L\alpha$, Ce$L\alpha$, Pr$L\beta$, Nd$L\alpha$, Sm$L\alpha$, Gd$L\beta$, Er$L\alpha$, Yb$L\alpha$), Mn-hortonolite (Mn$K\alpha$, Fe$K\alpha$), diopside (Mg$K\alpha$), wollastonite (Ca$K\alpha$), Pb (Pb$M\alpha$), Amelia albite (Na$K\alpha$), Asbe K-feldspar (K$K\alpha$), CaF_2 (F$K\alpha$) and Cl apatite (Cl$K\alpha$) (cf. Drake and Weill, 1972; Roeder, 1985; Jarosevich, 2002).

UNCORRECT PROOF

5. Rare accessory minerals

5.1. U—Th-bearing minerals (uraninite-thorianite, thorite)

U—Th minerals are represented by uraninite-thorianite (UO_2—ThO_2) and thorite (Th, U SiO_4; Table 3), ranging in size from 1 to 10 μm. SEM images are shown in supplementary materials (S1 and S2).

Thorianite has ThO_2 contents from 65 to 87 wt%, whereas UO_2 in uraninite grains varies between 83 and 89 wt% (Fig. 6A). Thorite, a rare nesosilicate of thorium that crystallizes in the tetragonal system, on the other hand, is isomorphous with zircon and contains high ThO_2 (from 43 to 55%) and low UO_2 (1.6–2.3%) contents. Yttrium and rare earth elements (REE), mostly Ce, may substitute for Th in amounts up to 8 wt% (Fig. 6B). As a matter of fact, the Y_2O_3+REE content is up to about 5 wt% in thorianite and up to about 11 wt% in thorite of Cerro Boggiani. It should be also noted that thorianite compositions reported in Table 3 are similar to those found in carbonatites worldwide (cf. Moine et al., 1998), suggesting the influence of deuteric-metasomatic fluids deriving from a carbonatitic magma.

Table 3
Representative analyses of uraninite, thorianite and thorite from Cerro Boggiani. Atoms per formula unit calculated on the basis of 4 oxygens.

Sample	RP28	RP31	RP36	RP38	RP28	RP36
	Uraninite		Thorianite		Thorite	
SiO_2	nd	0.15	0.92	0.90	21.15	22.40
TiO_2	nd	0.53	0.41	0.70	2.48	7.03
ZrO_2	nd	0.71	0.20	0.01	3.12	1.69
Nb_2O_5	nd	–	0.09	0.02	0.80	2.19
Ta_2O_5	nd	–	<0.19	0.01	0.02	0.02
WO_3	nd	–	<0.22	nd	0.00	0.27
Al_2O_3	nd	0.06	0.41	0.06	0.76	3.69
Y_2O_3	nd	0.09	<0.06	0.05	0.33	7.19
La_2O_3	nd	0.03	0.60	0.21	1.84	0.20
Ce_2O_3	0.28	0.01	2.60	0.45	2.16	0.53
Pr_2O_3	nd	0.01	<0.19	0.06	0.17	0.12
Nd_2O_3	0.12	0.03	0.64	0.18	0.40	0.51
Sm_2O_3	0.18	0.08	<0.10	0.03	0.05	0.33
Gd_2O_3	0.26	0.05	<0.20	0.02	0.06	0.98
Er_2O_3	0.10	0.01	<0.26	0.01	0.00	0.80
Yb_2O_3	0.14	0.01	<0.13	0.01	0.08	0.22
ThO_2	9.77	0.17	86.52	64.80	55.02	42.70
UO_2	82.71	89.08	3.94	25.00	2.26	1.61
Fe_2O_3	<0.05	0.33	0.32	1.53	0.31	3.01
MnO	<0.01	0.01	<0.07	0.05	0.06	0.70
MgO	<0.02	0.01	<0.03	<0.01	0.00	0.15
SrO	<0.02	–	<0.04	nd	0.12	0.06
CaO	0.08	1.48	0.34	0.21	2.47	2.57
PbO	3.95	1.60	1.01	3.81	0.11	0.04
Na_2O	<0.03	–	0.12	0.10	0.08	0.60
K_2O	<0,01	–	<0.03	0.10	0.10	0.12
BaO	<0.02	–	<0.12	nd	0.06	0.11
F	<0.11	–	0.17	nd	0.41	0.32
Sum	98.67	94.45	99.30	98.32	94.42	100.27
Atoms						
Si	–	0.014	0.077	0.074	1.015	0.910
Ti	–	0.034	0.025	0.042	0.088	0.176
Zr	–	0.030	0.008	–	0.073	0.032
Nb	–	–	0.004	–	0.017	0.038
Ta	–	–		–	0.001	0.000
W	–	–		–	0.000	0.003
Al	–	0.003	0.040	0.06	0.043	0.171
REE + Y	0.090	0.009	0.135	0.055	0.091	0.212
Th	0.201	0.004	1.633	1.215	0.601	0.398
U	1.683	1.728	0.073	0.441	0.024	0.015
Fe	–	0.022	0.020	0.104	0.011	0.085
Mn	–	–	0.005	–0.003	0.002	0.025
Mg	–	–	–	–	–	0.009
Sr	–	–	0.001	–	0.003	0.001
Ca	–	0.134	0.030	0.018	0.127	0.110
Pb	0.097	0.122	0.022	0.084	0.001	0.000
Na	–	–	0.019	0.014	0.007	0.044
K	–	–		0.010	0.006	0.002
Ba	–	–		–	0.001	0.002
Sum	2.071	2.100	2.092	2.066	2.111	2.233

5.2. Nb-bearing minerals (pyrochlore)

Pyrochlore is the main Nb-bearing mineral phase (oxide) present in the Cerro Boggiani rocks. This mineral is commonly associated with late-stage magmatic to deuteric processes and carbonate-fluorite veins, most probably of metasomatic origin (Torro et al., 2012 and references therein). Notably, in carbonatites, pyroclore is a common phase (Hogarth, 1989; Hogarth and Horne, 1989), represented by a group including cubic Nb—Ta—Ti oxides expressed by the structural formula $A_{16-x}B_{16}O_{48}(O,OH,F)_{8-y}{*}zH_2O$, where x and y are vacant sites in the unit cell (cf. Zurevinski and Mitchell, 2004 and references therein). Pyrochlore structures may accommodate a wide variety of cations, with A-site potentially occupied by As, Ba, Bi, Ca, Cs, K, Mg, Mn, Na, Pb, Y, REE, Sb, Sr, Th and U, and the B-site containing Nb, Ta, Ti, V, Al, Si, Fe and Zr.

Notably, the A-sites from the Cerro Boggiani pyrochlores are mainly characterized by Ca (0.51–1.13 a.f.u.), Na (0.19–0.96 a.f.u.) and REE (Ce from 0.14 to 0.23 a.f.u.) (Table 4, Fig. 7A). The minerals occur in contact with other phases as shown in S3 and fall into the pyrochlore field of the Ti—Nb—Ta classification diagram (Fig. 7B). According to the Ca—Na-$A_{vacancies}$ plot (Zurevinski and Mitchell, 2004 and references therein) in Fig. 7C, selected analyses of pyrochlore from phonolites (RP31 and RP41) and a nepheline syenite (RP38) may be considered to derive from both magmatic and hydrothermal crystallization. Indeed, pyrochlore crystals often show euhedral habits and should have mainly formed interstitially during late-stage magmatic to deuteric crystallization (e.g. Ridolfi et al., 2003, 2006).

This is supported by the analyses of substitutions (i) $^{A}Na^{Y}F \rightarrow {}^{A}\Upsilon^{Y}\Upsilon$, (ii) $^{A}Ca^{Y}O \rightarrow {}^{A}\Upsilon^{Y}\Upsilon$ (Υ = vacancies) and (iii) $^{A}Ca^{X}O \rightarrow {}^{A}\Upsilon^{X}\Upsilon$ in the representative pyrochlores (Fig.7). In fact, Lumpkin and Ewing (1995) recognized three types of alterations of the pyrochlore subgroup in nepheline syenites and carbonatites: primary alteration (i.e. hydrothermal), represented by the substitutions $^{A}Na^{Y}F \rightarrow {}^{A}\Upsilon^{Y}\Upsilon$ and $^{A}Ca^{Y}O \rightarrow {}^{A}\Upsilon^{Y}\Upsilon$ (Υ = vacancies) promoted by a fluid-phase at ~300–550 °C; secondary alteration (<150 °C, i.e. near surface, supergene), characterized by the same replacement reactions plus $^{A}Ca^{X}O \rightarrow {}^{A}\Upsilon^{X}\Upsilon$, and extreme hydration (10–15 wt% H_2O or 2–3 molecules pfu); and finally, transitional alteration (200–350 °C), in between the above two types of substitutions. According to the considerations above, the alteration patterns of the Cerro Boggiani pyrochlores (Fig.7) suggest that they underwent mostly primary and hydrothermal (transitional) alterations by high temperature (≥200 °C) F-rich fluids. In conclusion, pyrochlore from Cerro Boggiani agpaitic rocks are both of late-stage magmatic and deuteric origin (*sensu* Mitchell, 2015), containing more A-site cations than supergene (wheatering) pyrochlore, the latter being dominated by A-site vacancies and water.

5.3. REE-bearing minerals

REE-rich minerals are represented by a large number of crystalline phases (from S4 to S9): carbonates (burbankite-remondite), fluorcarbonates (bastnäsite-parisite-synchysite, cordylite), hydrate

UNCORRECTED PROOF

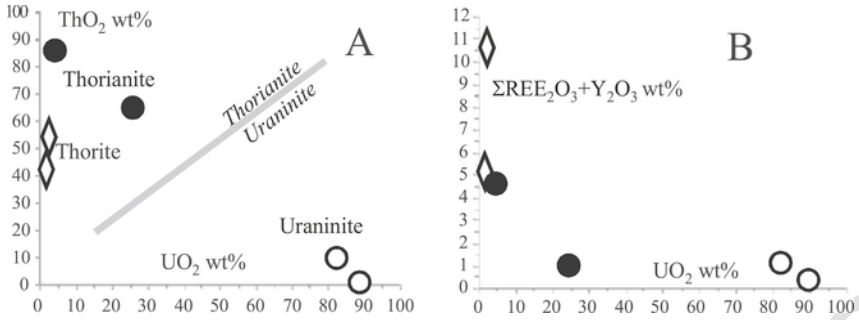

Fig. 6. UO_2 vs. ThO_2 (A) and UO_2 vs. ΣREE + Y_2O_3 (B) of thorianite, uraninite and thorite crystals from the Cerro Boggiani complex (after Förster, 1999 and references therein).

carbonates (ancylite, galgenbergite), phosphates (monazite) and silicate/phosphates (britholite). Carbonate, fluorcarbonate and hydrate carbonate phases from Cerro Boggiani have been the subjects of systematic investigations in the last decade (see e.g. Enrich et al., 2010).

5.3.1. Carbonates: burbankite (remondite)

The burbankite group is a rare strontium and cerium carbonate mineral (hexagonal) consisting of species with the general formula $A_3B_3(CO_3)_5$, where A = Na > Ca, REE and B = Sr, Ca, Ba, REE, Na (Belovtiskaya and Pekov, 2004 and references therein). Some crystals believed to be burbankite in the past, have now been identified as a new species called remondite (S4), which has a similar chemistry but monoclinic symmetry (Cesbron et al., 1988; Pekov et al., 2000). Representative chemical analyses are reported in Table 5 and SEM images are shown in S4 and S7.

Table 5 indicates that the dominant element in A-site is Na (2.17–3.0 a.f.u.), whereas the B-site contains various elements, i.e. Ca from 0.52 to 0.93 a.f.u., Sr from 0.22 to 1.26 a.f.u. and REE from 0.36 to 1.90 a.f.u.. Overall, the Cerro Boggiani burbankite (and remondite) plots in the field of the hydrothermalites (Fig. 8A) from nepheline syenite massifs at relatively low temperature, e.g. 250-100 °C, according to the CO_2 regime (cf. Belovtiskaya and Pekov, 2004; see also Fig. 5).

5.3.2. Fluorcarbonates: bastnäsite-parisite-synchysite series

The REE fluorcarbonates (Table 6) occur in significant amounts in the Cerro Boggiani minerals, for a total abundance of about 1 wt%. In particular, the bastnäsite-parisite-synchysite series (S2, S5 and S7) are typically found as fine-scale, complex intergrowths of fibroradial to plumose aggregates in which bastnäsite and synchysite are dominant over parisite.

They show textures similar to the fluorcarbonate minerals described in Ruberti et al. (2008) and Ridolfi et al. (2006) for the Barra do Itapirapuã carbonatites and Kilombe alkali feldspar syenites. The three minerals show similar compositions [i.e.: bastnäsite (Ca, La)(CO_3)F; parisite $Ca(Ce,La)_2(CO_3)_2F_2$; synchysite $Ca(Ce,La)(CO_3)_2F$], but are easily distinguished in the Σ(Ca + Sr) vs. ΣREE diagram (Fig. 8B).

A comparison with other Brazilian occurrences indicates conditions, for the formation of the Cerro Boggiani fluorcarbonate mineral associations, at temperatures between 375 and 80 °C (cf. Ruberti et al., 2008). It is worth noting that an origin of such fluorcarbonates from deuteric to metasomatic carbonatitic fluids is also suggested by the occurrence of thick intergrowths and corrosion phenomena among members of the series, as described by Ridolfi et al. (2006).

5.3.3. Fluorcarbonates: cordylite

Following Mills et al. (2012), cordylite, a Ba-fluorcarbonate, mainly occurs in metasomatic carbonate veins of the Biraya Fe-REE deposit (Irkutsk, Russia) closely associated with barite, biraite-(Ce), niobium-rich chevkinite-(Ce), fergusonite-(Nd), ancylite, bastnäsite, hydroxylbastnäsite-(Ce), monazite-(Ce), talc, humite, thorite, pyrite, and pyrrhotite. In the phonolite dyke RP28 of Cerro Boggiani, a very fine-grained vein consists mainly of carbonates (not analysed) with single grains of cordyilite-(Ce—La), together with ancylite, bastnäsite, parisite, synchysite, låvenite, thorite and pyrochlore (S6).

The ideal formula of cordylite is $(Na_{1-x}Ca_{x/2})BaREE_2(CO_3)_4F$, with $0 < x < 1$. It was redefined and simplified by Giester et al. (1998) to $NaBaCe_2(CO_3)_4$. In the Cerro Boggiani rocks, the cordylite composition (Table 6) roughly corresponds to the ideal formula proposed by Mills et al. (2012).

5.3.4. Hydrate carbonates: ancylite and galgenbergite

Microprobe analyses of ancylite and galgenbergite are reported in Table 7 (see also S3, S6, and S8) and represented in the REE-Sr-Ca diagram of Fig. 9.

Ancylite [ideal formula $SrCe(CO_3)_2(OH)\cdot(H_2O)$, according to Pekov et al., 1997] from Cerro Boggiani shows REEs between 1.12 and 1.33 a.f.u., with prevailing Ce (0.54–0.70) and La (0.42–0.44), and subordinate Nd (0.10–0.12). Sr (0.46–0.54 a.f.u.) prevails over Ca (0.24–0.34), defining the field of ancylite s.s. (see Pekov et al., 1997). The anionic group includes OH^- (4.3–4.6 wt%) and CO_3^{2-} (22.5–23.5 wt%) and shows fluorine contents of 0.81–0.86 wt%, corresponding to 0.18 a.f.u. (cf. Zaitsev et al., 1998).

Galgenbergites, with a simplified formula $Ca(Ce,La)_2(CO_3)_4{*}H_2O$ according to Walter et al. (2013), occasionally occur in the Cerro Boggiani rocks (samples RP27 and RP36, Table 7). Considering a structural formula on the basis of 8 CO_3, Cerro Boggiani galgenbergites have REE contents of 3.6–3.7 a.f.u., Ca > Sr and Ca + Sr between 1.57 and 1.97 a.f.u..

5.3.5. Phosphates: monazite

Monazite, [$(Ce,La,Nd,Th)PO_4$], represents one of the most common REE and Th-rich accessory minerals (cf. Toledo and Pereira, 2003; Williams et al., 2007; Harlov and Hetherington, 2010 and references therein). The tetrahedral site of Cerro Boggiani monazites (Table 8) is dominated by P (3.4–3.7 a.f.u.) and includes Si (0.2–0.4 a.f.u.) and Al (0.1–0.2 a.f.u.). By contrast, the polyhedrons (coordination 9, according to Niet et al., 1995, and to Clavier et al., 2011) are largely occupied by REE + Y (3.5–4.0 a.f.u.) with Ce > La (1.9 vs. 1.1–1.8 a.f.u., respectively); notably, Th ranges from 0.02 to 0.22 a.f.u.. Overall, the Th + U and REE + Y + P are in the ranges of 0.60–0.18 and 6.90–7.75 a.f.u., respectively.

5.3.6. Phosphates/silicates: britholite

Britholite (S9), a basic phosphate/silicate mineral of sodium, calcium and Ce [$(Ca,Na)_3Ce_2(SiO_4)_2(PO_4)F$, according to Oberti et al. (2001) and Pekov et al. (2007)], is a very rare accessory phase in the

UNCORRECTED PROOF

Table 4
Representative chemical analyses of pyrochlore from the Cerro Boggiani complex. Structural formula calculated on the basis of 2-B site cations (cf. Chakhmouradian and Mitchell, 1998); R = rim.

Rock-type	Phonolite lava flow	Phonolite lava flow	Nepheline syenite	Nepheline syenite	Nepheline syenite	Nepheline syenite	Nepheline syenite	Phonolite lava flow	Phonolite lava flow	Phonolite lava flow	Phonolite lava flow	Phonolite lava flow	Phonolite lava flow
Sample	RP31A	RP31BR	RP38B-1	RP38B-2	RP38B-3	RP38B-4 R	RP38B-5 R	RP41-1	RP41-2	RP41-3	RP41-4	RP41-5	RP41-6 R
SiO_2	1.41	0.00	4.18	3.27	0.73	3.86	3.39	4.87	3.34	9.38	1.41	2.16	0.00
TiO_2	9.50	2.61	8.81	9.29	9.12	10.01	9.42	4.59	4.69	3.78	3.02	3.57	3.33
ZrO_2	5.91	2.45	1.34	1.13	1.71	0.29	0.22	2.64	1.24	4.58	2.85	2.97	3.55
Nb_2O_5	35.64	45.53	52.90	54.63	56.39	47.84	48.44	51.71	53.28	46.80	55.09	57.01	50.54
Ta_2O_5	6.48	11.72	1.38	1.22	1.13	1.38	1.76	1.47	1.53	2.57	1.78	1.10	9.56
WO_3	–	–	<0.19	0.21	0.54	<0.19	<0.19	1.15	2.04	<0.19	0.81	0.72	–
Al_2O_3	0.01	0.06	0.07	0.06	0.03	0.44	0.57	1.07	1.98	0.14	4.67	0.09	0.03
Y_2O_3	–	–	0.09	<0.05	<0.05	<0.05	<0.05	<0.05	<0.05	<0.05	<0.05	<0.05	0.03
La_2O_3	1.35	0.08	0.27	0.41	1.65	1.42	1.60	1.81	2.01	0.98	2.46	2.23	0.13
Ce_2O_3	9.77	0.41	0.67	0.70	3.50	2.02	2.10	4.10	4.62	2.02	5.52	4.62	0.79
Pr_2O_3	0.60	0.02	0.21	0.19	0.40	0.18	0.26	0.29	0.38	<0.16	0.38	0.31	0.03
Nd_2O_3	1.94	0.03	0.29	0.26	0.72	0.38	0.35	0.85	1.02	0.37	1.02	0.86	0.14
Sm_2O_3	0.21	–	<0.08	<0.08	<0.08	<0.08	0.09	0.13	0.19	<0.08	0.14	0.13	–
ThO_2	1.99	1.88	0.51	0.33	0.24	1.32	0.94	0.39	0.64	0.08	0.37	0.34	2.29
UO_2	6.37	14.32	0.11	<0.06	0.09	2.04	2.09	0.08	<0.06	0.07	<0.06	<0.06	8.84
FeO	1.71	1.25	0.50	0.26	0.15	1.45	1.62	0.13	0.75	0.14	0.15	0.14	1.07
MnO	–	0.03	0.44	0.29	0.27	0.43	0.41	0.83	0.76	0.38	0.07	0.17	0,03
MgO	–	0.07	<0.02	<0.02	<0.02	0.06	0.04	<0.02	<0.02	<0.02	<0.02	<0.02	0.09
SrO	–	0.55	0.43	0.66	0.46	0.71	0.90	0.27	0.17	0.30	0.31	0.33	0.62
CaO	16.26	8.73	14.35	15.71	13.70	10.64	10.78	9.69	8.34	10.57	9.13	10.39	8.08
PbO	–	0.65	<0.10	<0.10	<0.10	0.18	0.15	<0.10	<0.10	<0.10	<0.10	<0.10	0.42
Na_2O	1.53	0.15	6.53	6.54	5.88	1.97	1.89	6.21	6.95	7.69	7.63	8.08	0.48
K_2O	–		0.17	0.14	0.08	0.20	0.23	0.68	0.65	0.59	0.04	0.07	
BaO	–	0.61	0.11	0.14	<0.10	0.13	<0.10	<0.10	<0.10	<0.10	<0.10	<0.10	0.71
F	nd	1.06	5.01	4.79	5.15	0.62	0.78	3.05	3.68	4.30	4.55	4.97	1.52
$\overline{\overline{=}}O$ $=F$	–	0.40	2.11	2.02	2.17	0.26	0.33	1.28	1.55	1.81	1.92	2.09	0.62
Sum	100.68	92.61	96.46	98.51	99.88	87.54	87.92	94.98	96.87	93.21	99.60	98.21	91.68
B-site													
Nb	1.048	1.462	1.334	1.373	1.482	1.268	1.302	1.338	1.383	1.159	1.377	1.578	1.491
Ta	0.115	0.243	0.021	0.018	0.018	0.022	0.028	0.023	0.024	0.038	0.027	0.018	0.171
Ti	0.465	0.133	0.370	0.389	0.399	0.442	0.421	0.198	0.202	0.156	0.125	0.164	0.164
Si	0.092	–	0.233	0.182	0.042	0.227	0.201	0.279	0.192	0.514	0.078	0.132	–
Zr	0.187	0.084	0.036	0.031	0.048	0.008	0.006	0.074	0.035	0.122	0.077	0.089	0.113
W	–	–	0.001	0.003	0.008	0.002	0.001	0.017	0.030	0.002	0.012	0.011	–
Al	–	0.003	0.005	0.004	0.002	0.031	0.040	0.072	0.134	0.009	0.304	0.006	0.002
Fe	0.093	0.075	–	–	–	–	–	–	–	–	–	–	0.059
Sum B	2.000	2.000	2.000	2.000	2.000	2.000	2.000	2.000	2.000	2.000	2.000	2.000	2.000
A-site													
Ca	1.133	0.629	0.858	0.936	0.853	0.669	0.687	0.594	0.513	0.620	0.541	0.682	0.566
La	0.032	0.002	0.006	0.008	0.035	0.031	0.035	0.038	0.042	0.020	0.050	0.050	0.003
Ce	0.233	0.011	0.014	0.014	0.075	0.043	0.046	0.086	0.097	0.041	0.112	0.104	0.019
Pr	0.014	0.000	0.004	0.004	0.008	0.004	0.006	0.006	0.008	0.001	0.008	0.007	0.001
Nd	0.042	0.001	0.006	0.005	0.015	0.008	0.007	0.017	0.021	0.007	0.020	0.019	0.003
Sm	–	–	0.001	0.001	0.001	0.001	0.002	0.003	0.004	0.000	0.003	0.003	–
Th	0.029	0.031	0.007	0.004	0.003	0.018	0.013	0.005	0.008	0.001	0.005	0.005	0.034
U	0.092	0.229	0.001	0.001	0.001	0.027	0.028	0.001	0.000	0.001	0.000	0.001	0.130
Mn	–	0.002	0.021	0.014	0.013	0.021	0.021	0.040	0.037	0.018	0.003	0.009	0.002
Mg	–	0.007	0.000	0.000	0.000	0.005	0.004	0.001	0.002	0.000	0.001	0.002	0.002
Sr	–	0.024	0.014	0.021	0.015	0.024	0.031	0.009	0.005	0.010	0.010	0.012	0.023
Pb	–	0.013	0.000	0.000	0.000	0.003	0.002	0.000	0.001	0.000	0.000	0.000	0.008
Na	0.193	0.020	0.707	0.705	0.663	0.224	0.218	0.689	0.774	0.817	0.818	0.959	0.061
K	–	–	0.012	0.010	0.006	0.015	0.017	0.050	0.048	0.041	0.003	0.006	–
Ba	–	0.016	0.002	0.003	0.000	0.003	0.002	0.001	0.000	0.000	0.001	0.000	0.018
Sum A	1.768	0.905	1.679	1.742	1.698	1.167	1.201	1.553	1.598	1.584	1.582	1.864	0.870
F	–	0.233	0.884	0.843	0.946	0.115	0.146	0.552	0.669	0.744	0.796	0.963	0.313

Cerro Boggiani rocks and shows Ca < ΣREE (i.e. 3.3 vs. 5.5 a.f.u.) with Ce = 2.6 and Ce/La = 1.02 a.f.u.. The tetrahedral site contains 4.9 and 0.9 a.f.u. of Si and P, respectively (Table 8; cf. S9, associated to monazite). By contrast, the anionic site is characterized by F = 2.64 a.f.u. (cf. chemical composition of britholite from the Monte de Trigo Island nepheline syenites from Enrich and Ruberti, 2004). According to Andersen (2014, and references therein), monazite and britholite are stable at relatively high and low silica activities respectively, which is compatible with britholite occurrence in silica-undersaturated rocks.

5.4. Zr-rich silicate minerals

Zr-rich silicate phases of the Cerro Boggiani rocks are represented by rosenbuschite and låvenite (cuspidine-wöhlerite group), and eudialyte with subordinate catapleiite (Carbonin et al., 2005;

UNCORRECTED PROOF

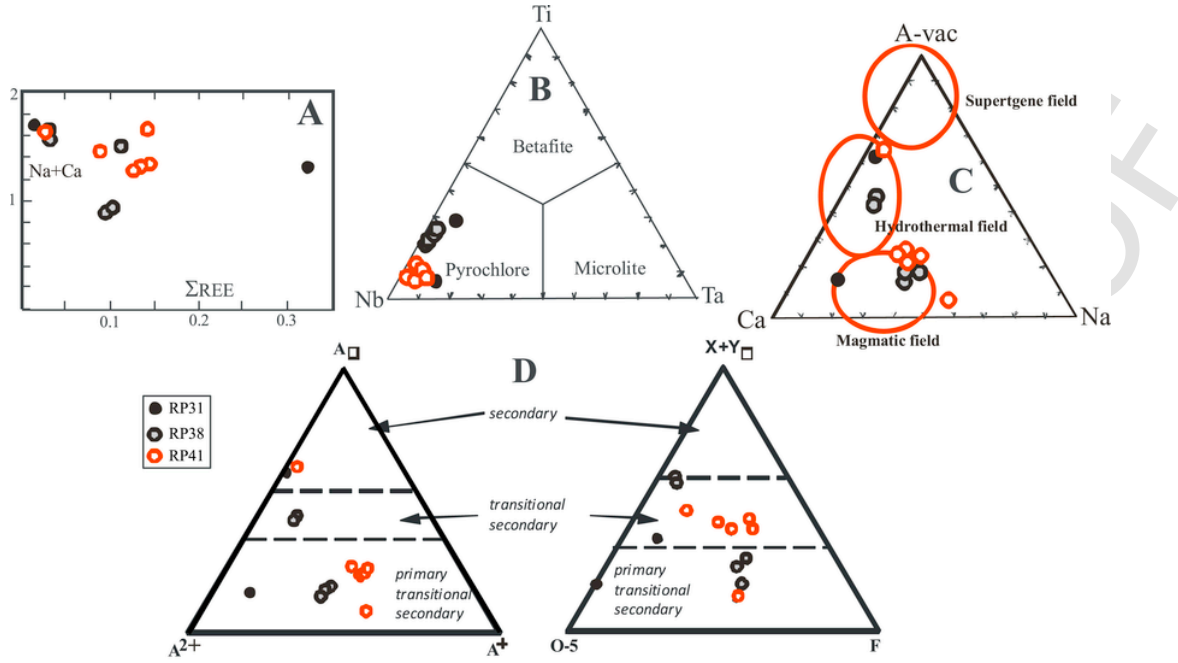

Fig. 7. A: Na + Ca (a.f.u.) vs. REE for pyrochlore samples. **B**: Ti—Nb—Ta pyrochlore compositional diagram (cf. Hogarth and Horne, 1989 and references therein). **C**: Ca—Na-$A_{vacancies}$ plot showing representative compositions of pyrochlore from Cerro Boggiani. The fields are after Zurevinski and Mitchell (2004 and references therein). **D**: Triangular plots showing the atomic percentage variations of A-site vacancies ($^{A}\Upsilon$), X + Y anion vacancies ($^{X+Y}\Upsilon$), divalent and monovalent A-site cations (A^{2+} and A^{+}), oxygen (plotted as O-5) and fluorine (F) in the Cerro Boggiani pyrochlores. The maximum amount of vacancies due to primary (T ca. 300–550 °C), transitional (T ca. 200–300 °C) and secondary (T < 150 °C) alterations are also reported; after Lumpkin and Ewing (1995).

Comin-Chiaramonti et al., 2005; Enrich et al., 2011, 2012). Chemical analyses are reported in Table 9 (cf. also Fig. 2). As described by Carbonin et al. (2005), rosenbuschite and låvenite are disilicates characterized by tetrahedra pairs (Si_2O_7) and by octahedral cations, varying from small-radius and high charge, i.e. Ti^{4+}, Zr^{4+} and Nb^{5+} to Mn^{2+} and Fe^{2+}, and larger-radius, low charge Na^{+} and Ca^{2+} (Bellezza et al., 2003; Ridolfi et al., 2003). By contrast, eudialyte is a ring silicate, represented by a Na-rich zirconosilicate characterized by both three and nine-membered rings of SiO_4 tetrahedra. Moreover, the mineral chemistry of these phases (Table 9; Fig.10) emphasizes high concentrations of MnO (i.e. rosenbuschite 2.8 wt%, låvenite 6.0 wt% and eudialyte 4.8 wt%; Table 9). In particular, Mn-rich eudialyte is considered as indicative of a postmagmatic/deuteric stage of crystallization (Aksenov et al., 2014).

5.4.1. Rosenbuschite

In the rosenbuschite group ($Na_6Ca_6Zr_3Ti(Si_2O_7)_2\ O_2F_2$), the polyhedra combine into layers (*O* layers) and into ribbons by edge sharing. Heterogeneous layers (*H* layers) composed of the octahedra from the ribbons and the sorosilicate groups alternate with the *O* layer into a layered *HOH* structure (cf. Bellezza et al., 2003; Carbonin et al., 2005).

Although it shows MnO content between 2.7 and 2.9 wt% (Table 9), rosenbuschite from Cerro Boggiani (Fig. 2A–D) is consistent with the above crystal chemistry. This MnO abundance is significantly higher than typical rosenbuschite (e.g. from the Langesundfjord nepheline syenites in Norway) but similar to that found in Zaangar'ya rocks in Russia (Deer et al., 1997), as already noticed by Carbonin et al. (2005).

5.4.2. Låvenite

The analyses of the Cerro Boggiani låvenite yield the following crystal chemical formula, calculated on the basis of 9(O,F):

$$(Na_{1.34}Ca_{0.66})_{2.00}(Mn_{0.38}Fe_{0.22}Mg_{0.01}Ti_{0.16}Ca_{0.18})_{0.95}$$

$$(Zr_{0.74}Ti_{0.16}Nb_{0.10})_{1.00}(Si_{1.97}O_{7.00})O_{0.88}F_{1.12}$$

which is particularly close to the comprehensive chemical formula suggested by Mellini (1981), i.e. $W_2XY(Si_2O_7)O(O,OH,F)$,where W = Na,Ca; X = Mn,Fe,Mg,Ti and some Ca; Y = Zr,Ti,Nb,Ta (cf. also Carbonin et al., 2005). As a matter of fact, the point analyses are in the låvenite field (Fig. 10A, B).

Similarly to the rosenbuschite, the high Mn concentration of the låvenite is noteworthy (up to 6 wt%) and comparable to that of the same phase in the Junguni nepheline syenites from Malawi (Woolley and Platt, 1988), as previously observed by Carbonin et al. (2005).

5.4.3. Eudialyte and Ca-catapleiite

The Na-rich zirconosilicate eudialyte from the Cerro Boggiani (Fig. 2) has the following formula (see Johnsen and Grice, 1999 for calculation):

$$(Na_{10.85}Ca_{1.70}K_{0.19}Sr_{0.10}La_{0.13}Ce_{0.08})_{13.05}(Ca_{4.90}Mn_{1.10})_{6.00}$$

$$(Fe_{2.02}Mn_{0.96}Mg_{0.02})_{3.00}Zr_{3.00}$$

$$(Nb_{0.39}Ti_{0.20}Zr_{0.09}Si_{0.33})_{1.01}Si_{24.96}Al_{0.04}O_{74.23}Cl_{1.13}$$

It indicates a cation deficiency in the Na sites. Notably, the calculated eudialyte analyses allow the mineral to be placed between eudialyte s.s. and a REE rich type (cf. Sjöqvist et al., 2013). The eudi-

UNCORRECTED PROOF

Table 5
Representative chemical analyses of burbankite (RP28, RP31 and RP38) and remondite (RP33 and RP41) from Cerro Boggiani. Atoms per formula unit based on 6 cations.

Sample	RP28	RP31	RP33	RP38	RP41
CaO	8.63	13.46	7.83	7.62	4.20
SrO	16.70	19.42	3.46	9.37	3.68
BaO	1.58	13.56	0.09	4.40	1.23
La_2O_3	15.24	2.34	15.85	13.42	18.04
Ce_2O_3	14.20	4.65	15.83	15.22	21.01
Pr_2O_3	0.78	0.37	1.21	1.22	1.97
Nd_2O_3	2.17	1.40	2.80	2.91	4.04
Sm_2O_3	0.15	0.10	0.43	0.29	0.45
Gd_2O_3	0.04	0.08	0.12	0.09	0.13
Er_2O_3	0.02	–	0.03-	0.03	0.05
Yb_2O_3	0.01	–	–	–	–
Y_2O_3	0.02	0.10	0.12-	0.04	0.12
Na_2O	12.74	9.69	16.32	12.99	14.76
CO_2	27.55	33.32	34.11	32.22	29.90
Sum	99.83	98.16	99.31	99.82	99.50
Atoms					
Na	2.643	2.166	3.000	2.847	3.000
Ca	0.357	0.834	–	0.143	–
Sum A	3.000	3.000	3.000	3.000	3.000
Na	–	–	0.394	–	0.289
Ca	0.628	0.777	0.925	0.751	0.516
Sr	1.033	1.255	0.216	0.695	0.245
Ba	0.060	0.603	–	0.188	0.044
La	0.599	0.095	0.625	0.557	0.765
Ce	0.554	0.191	0.627	0.627	0.882
Pr	0.030	0.015	0.05	0.042	0.062
Nd	0.082	0.055	0.105	0.118	0.166
Sm	0.011	0.005	0.01	0.011	0.017
Gd	0.001	0.003	–	0.004	0.005
Er	0.001	–	–	0.001	0.002
Y	–	–	0.010	0.005	0.007
Sum B	2.999	3.000	2.952	3.000	3.000

alyte compositions of Cerro Boggiani closely match those of the silica-undersaturated syenite nodules of Agua de Pau (Azores, Ridolfi et al., 2003).

Ca-catapleiite, typically formed as the result of metasomatic alteration of eudialyte (Karup-Møller et al., 2010 and references therein; Fig. 2) shows a more simplified composition, approximately $CaZrSi_3O_9 2H_2O$ (cf. Table 8 and Merlino et al., 2004).

6. Discussion and conclusions

Electron microprobe analyses of accessory minerals in the nepheline syenite and phonolite rock-types from the Cerro Boggiani agpaitic complex (Alto Paraguay) confirm the presence of several phases enriched in U—Th (uraninite-thorianite and thorite), Nb (pyrochlore), REEs (burbankite, bastnäsite-parisite-synchysite, cordylite, ancylite and galgenbergite, monazite and britholite) and Zr (rosenbuschite, låvenite and eudialyte). It is worth noting that these minerals usually crystallize at late magmatic and deuteric conditions (cf. Ruberti et al., 2008; Enrich et al., 2010 and references therein). In addition, the high content of volatiles (e.g. CO_2, F, Cl and H_2O) and incompatible elements in the Cerro Boggiani complex is typical of agpaitic and carbonatitic magmas (cf. Kogarko et al., 1974, 1977; Kogarko, 1987; Woolley and Platt, 1988; Sørensen, 1997; Ruberti et al., 2008), not only related to a deuteric stage of crystallization but also to metasomatic mineralizing fluids, mainly giving rise to crystallization of accessory fluorcarbonates and hydrate carbonates. Among the hydrothermal fluids which affected the Cerro Boggiani nepheline syenites and phonolites, a qualitatively distinction between those with $H_2O > CO_2$ (deuteric *stricto sensu*) and $CO_2 \geq H_2O$ (metasomatic) can be considered. It is worth noting that the term deuteric refers to reactions between primary magmatic minerals and the water-rich solutions that separate from the same body of magma at a late stage in its cooling history. By contrast, metasomatic minerals relates to fluids percolating through the crystallizing body but coming from outside that magmatic system. In the present case study of Cerro Boggiani rocks the metasomatic fluids are inferred to be of carbonatitic origin.

The LREE to MREE spider diagram patterns (normalized to chondrites CI; Fig.11) of pyroclore and REE-bearing minerals can give additional petrologic information. It is worth noting that positive Ce-spikes are typically found in magmatic pyrochlores of carbonatites (Hogarth et al., 1988; Hornig-Kjarsgaard, 1998; Wagner et al., 2003) and pyrochlore Ce anomaly of Cerro Boggiani varies from slightly negative to positive (Ce/Ce* = 0.6–2.4). A similar feature is observed for a few Cerro Boggiani bastnäsite crystals showing Ce/Ce* values up to 5.1 (Fig.11). In these crystals, the positive Ce anomaly is mostly due to low REE contents (other than Ce) with respect to other bastnäsite-parisite crystals (Table 6).

The other REE-minerals show strongly fractionated chondrite-normalized LREE patterns and no significant Ce anomaly (Ce/Ce* = 0.8–1.6; Fig.11). The chondrite normalized La/Nd ratios is between 6 and 18, suggesting that mineralization is due to CO_2-rich metasomatic fluids. This inference is supported by studies of fluid inclusions in REE-minerals such as fluorite, monazite and bastnäsite-parisite (Smith et al., 2000). Smith et al. (2000) have shown that mineral REEs partitioning can be correlated with the composition and temperature of the mineralizing fluids. Due to the occurrence of REE complexes at low temperature and with H_2O-rich fluids, partitioning of rare earth elements typically increases with atomic number, leading to higher MREE solubility. Accordingly, the crystallization of REE–minerals with La/Nd_N ratios <2 takes places in dominant aqueous solutions at low temperatures (minimum estimates of 150–250 °C), whereas REE phases with $La/Nd_N > 4$

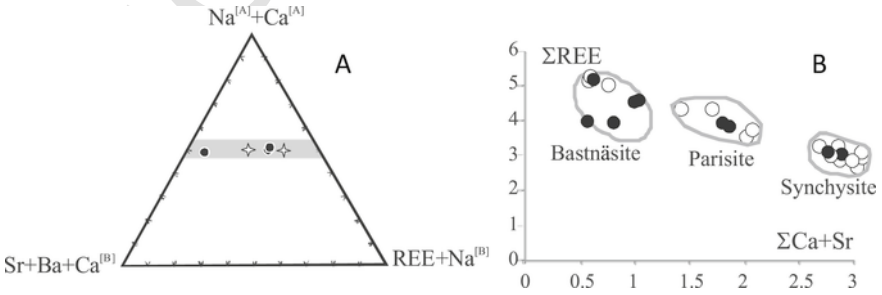

Fig. 8. A: Plot of the cation ratios for burbankites and remondites from Table 5 (full circles: burbankite s.s.; stars: remondite); the grey field represents burbankite group minerals linked to alkaline hydrothermalites of nepheline syenite massifs as reported by Belovtiskaya and Pekov (2004). **B**: (Ca + Sr) vs REE (a.f.u.) for bastnäsite, parisite and synchysite minerals; the fields are after Gieré (1996); full circles: this work; open circles: from Ruberti et al. (2008).

CORRECTED PROOF

Table 6
Representative compositions of fluorcarbonate minerals from Cerro Boggiani. Structural formulae calculated on the basis of six cations per formula unit; $(CO_3)^{2-}{}_{CALC}$ is calculated by charge balance.

Sample	Bastnäsite					Parisite		Synchysite		Cordylite
	RP28	RP31A	RP31B	RP36	RP38	RP28	RP31A	RP28	RP31A	RP28
SiO_2	3.07	–	0.74	0.33	0.30	0.06	0.08	0.05	0.04	–
Al_2O_3	0.79	0.01	0.04	0.76	–	0.44	0.99	0.04	0.03	–
Fe_2O_3	0.53	–	4.59	0.14	0.40	–	<0.05	–	–	0.11
Y_2O_3	0.45	0.58	0.44	–	1.70	0.26	0.27	0.38	0.48	0.44
La_2O_3	15.31	23.92	18.66	28.84	25.01	23.80	22.74	18.56	17.98	14.65
Ce_2O_3	39.05	30.05	28.90	28.79	30.91	28.25	27.53	25.26	24.73	22.82
Pr_2O_3	1.11	1.97	1.87	1.30	1.68	1.67	1.71	1.71	1.69	1.11
Nd_2O_3	3.24	6.24	5.59	3.22	4.56	4.65	5.06	5.46	5.67	3.04
Sm_2O_3	0.48	0.78	0.70	0.36	0.66	0.37	0.47	0.57	0.56	0.23
Eu_2O_3	–	0.30	–	–	0.52	0.18	0.16	0.17	0.19	–
Gd_2O_3	0.06	0.70	0.24	–	1.70	0.29	0.37	0.44	0.46	0.07
Dy_2O_3	0.06	0.21	–	–	0.31	0.09	0.10	0.13	0.15	0.06
ThO_2	1.90	2.60	4.65	0.58	0.24	3.04	3.87	2.48	3.87	2.69
UO_2	0.17	0.02	0.11	–	–	0.05	0.05	0.05	0.06	0.06
MnO	–	–	0.20	–	–	–	–	–	–	0.02
SrO	0.61	2.03	0.84	0.07	0.47	1.61	1.66	1.88	1.12	1.83
BaO	–	–	–	–	–	–	–	–	–	17.75
CaO	3.91	1.51	2.21	4.75	4.81	8.54	8.80	15.52	16.29	1.83
Na_2O	0.75	–	0.62	0.28	0.10	–	–	–	–	3.00
K_2O	0.15	–	0.07	0.03	–	–	–	–	–	0.06
F	5.57	8.63	6.22	6.79	6.66	8.35	8.44	8.70	9.08	2.43
Cl	0.05	–	–	0.03	–	–	–	–	–	–
$—O═F,Cl$	2.36	3.64	2.62	2.87	2.81	3.60	3.55	3.66	3.83	1.02
Sum	74.90	75.91	74.80	73.87	75.82	78.00	78.43	77.74	77.75	78.65
Atoms										
Ca	0.737	0.356	0.461	1.007	1.010	1.637	1.668	2.682	2.795	0.505
Sr	0.064	0.260	0.094	0.008	0.054	0.170	0.175	0.088	0.102	0.109
Ba							–	–	–	1.789
Na	0.265	–	0.233	0.106	0.038	–	–	–	–	0.497
K	0.035	–	0.018	0.008	0.004	–	–	–	–	0.019
Σ	1.101	0.616	0.806	1.129	1.106	1.807	1.843	2.770	2.897	2.999
Si	0.560	-	0.144	0.065	0.059	0.010	0.013	0.008	0.005	–
Al	0.170	-	0.010	0.177	0.004	0.093	0.124	0.004	0.004	-
Fe	0.073	–	0.672	0.020	0.059	–	–	–	–	0.021
Y	0.043	0.068	0.045	0.005	0.177	0.024	0.029	0.032	0.040	0.060
La	1.030	1.948	1.340	2.104	1.806	1.595	1.499	1.106	1.053	1.389
Ce	2.608	2.429	2.060	2.085	2.216	1.877	1.813	1.495	1.438	2.151
Pr	0.074	0.158	0.133	0.094	0.120	0.135	0.112	0.101	0.098	0.103
Nd	0.211	0.492	0.388	0.227	0.319	0.301	0.325	0.316	0.303	0.278
Sm	0.030	0.060	0.047	0.025	0.044	0.023	0.029	0.031	0.031	0.021
Eu	–	0.023	–	–	–	0.008	0.010	0.010	0.011	–
Gd	0.004	0.052	0.016	0.008	0.034	0.017	0.022	0.024	0.024	0.006
Dy	0.003	0.015	–	0.002	0.019	0.004	0.006	0.004	0.006	0.005
Th	0.078	0.130	0.206	0.026	0.011	0.125	0.159	0.090	0.118	0.160
U	0.013	0.002	0.005	–	0.003	0.002	0.003	0.001	0.001	0.004
Σ	4.897	5.377	5.066	4.811	4.871	4.214	4.158	3.222	3.139	4.198
F	3.213	6.027	3.832	4.250	4.125	4.924	4.810	4.439	4.545	1.972
Cl	0.015	–	–	0.009	–	–	–	–	–	–
$(CO_3)^{2-}{}_{CALC}$	6.252	6.073	6.464	6.308	6.363	6.068	6.007	6.049	6.063	8.008

should have originated from CO_2-rich fluids (with XCO_2 up to 0.84) (Smith et al., 2000; Ridolfi et al., 2006).

According to textural relationships and the overall mineral chemistry of the investigated accessory phases, coupled with compositional comparisons with the same mineral species in agpaitic-carbonatitic igneous complexes worldwide, a sequence of late accessory minerals of the Cerro Boggiani nepheline syenites and phonolites is emphasized. As shown in Fig. 12 the investigated rare accessory minerals of Cerro Boggiani can be distinguished in: 1) late-stage magmatic, 2) hydrothermal deuteric, and 3) hydrothermal metasomatic (carbonatitic fluids-related).

The deuteric stage of the agpaitic Cerro Boggiani nepheline syenites and phonolites was followed by the crystallization of some accessory minerals driven by carbonatitic fluids (Haas et al., 1995; Zaitsev et al., 1998). It is therefore inferred that CO_2-, F-, H_2O-, and LREE-rich carbonatitic fluids percolated through the subvolcanic system and interacted with the Cerro Boggiani peralkaline and agpaitic silicate melts during and shortly after their magmatic crystallization.

Uncited reference

Birkett et al., 1992, Mahato et al., 2013.

Acknowledgements

We would like to thank Brazilian agencies (FAPESP Proc. 2013/18073-4 and 2012/06082-6) for the financial support. Two anony-

UNCORRECTED PROOF

Table 7
Representative analyses of hydrate carbonates from Cerro Boggiani. Structural formulae for ancylite are calculated on the basis of two cations; calc.*, wt.%, calculated according to Dal Negro et al. (1975). Structural formulae for galgenbergite are based on ($8CO_3$), according to Walter et al. (2013).

Sample	Ancylite		Galgenbergite	
	RP30	RP38	RP27	RP36
Al_2O_3	0.27	0.17	0.48	1.20
Y_2O_3	–	–	0.05	0.01
La_2O_3	17.83	18.10	24.82	26.88
Ce_2O_3	23.47	29.05	22.53	23.86
Pr_2O_3	1.40	2.03	1.19	1.17
Nd_2O_3	4.18	4.96	3.05	2.88
Sm_2O_3	0.44	0.33	0.37	0.27
ThO_2	0.16	–	0.10	0.45
UO_2	–	–	0.06	0.02
Fe_2O_3	0.28	–	0.67	0.93
MnO	–	–	0.07	–
SrO	12.87	14.20	6.75	2.44
CaO	5.05	3.95	6.10	6.28
BaO	0.16	0.79	–	–
Na_2O	–	–	0.22	0.69
K_2O	0.09	–	–	0.05
F	0.81	0.86	0.93	0.92
Cl	–	–	–	0.01
$-O=F,Cl$	0.34	0.36	0.39	0.39
CO_2 calc*	23.51	22.53	29.96	29.31
OH calc*	4.64	4.33	–	–
H_2O calc*	3.94	3.82	2.29	2.23
Sum	101.23	98.51	99.94	98.92
Atoms				
Al	0.020	0.013	0.107	0.102
Y	–	–	0.005	0.001
La	0.421	0.440	1.728	1.685
Ce	0.538	0.702	1.557	1.698
Pr	0.033	0.049	0.082	0.082
Nd	0.096	0.117	0.206	0.199
Sm	0.010	0.007	0.024	0.018
Gd	0.003	0.003	0.001	0.001
Th	0.002	0.001	0.005	0.020
U	–	–	0.002	0.001
Fe	0.014	–	0.094	0.135
Mn	–	–	0.011	–
Sum	1.138	1.332	3.822	3.942
Sr	0.465	0.536	0.740	0.273
Ca	0.337	0.245	1.233	1.299
Ba	0.004	–	–	–
Sum	0.806	0.658	1.973	1.572
F	0.172	0.184	0.558	0.562

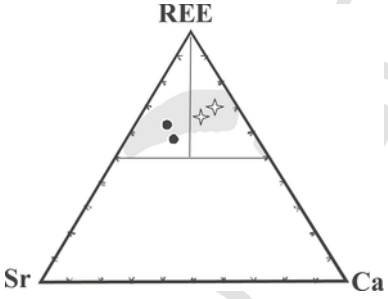

Fig. 9. REE-Sr-Ca variation diagram for ancylite (full circles) and galgenbergite (stars) from Cerro Boggiani samples (cf. Table 7). The grey field represents the composition of world-wide ancylites and Ca-ancylites after Pekov et al. (1997).

Table 8
Representative analyses of monazite (cations on the basis of 16 oxygens) and britholite (number of ions on the basis of 26 (O, F); according to Oberti et al. (2001).

Sample	Monazite		Britholite
	RP28	RP36	RP36
SiO_2	2.30	0.99	18.57
P_2O_5	23.85	28.06	4.17
Al_2O_3	0.82	0.46	0.45
Y_2O_3	0.42	–	0.04
La_2O_3	17.11	30.99	25.95
Ce_2O_3	31.24	33.33	26.65
Pr_2O_3	2.16	1.38	1.23
Nd_2O_3	5.64	3.55	2.88
Sm_2O_3	0.56	0.41	0.27
Gd_2O_3	0.25	0.06	–
ThO_2	5.75	0.61	3.23
UO_2	–	–	0.08
Fe_2O_3	–	–	0.58
MnO	–	–	0.28
SrO	0.69	0.09	0.35
CaO	2.02	0.34	11.84
Na_2O	0.47	–	0.41
K_2O	0.06	–	0.18
BaO	0.26	–	–
F	0.98	0.13	3.15
Cl	0.11	–	0.01
$-O=F,Cl$	0.44	0.05	1.33
Sum	94.35	100.45	98.99
Atoms			
P	3.381	3.729	0.912
Si	0.384	0.157	4.880
Al	0.163	0.091	0.135
Sum	3.928	3.977	5.927
Y	0.037	0.003	0.006
La	1.056	1.797	2.528
Ce	1.915	1.917	2.576
Pr	0.132	0.079	0.118
Nd	0.337	0.199	0.272
Sm	0.033	0.022	0.024
Gd	0.014	0.007	–
Th	0.219	0.022	0.188
Fe	–	–	0.113
Mn	–	–	0.059
Sr	0.067	0.009	0.054
Ca	0.362	0.059	3.332
Na	0.154	–	0.170
K	0.013	–	0.057
Ba	0.017	–	–
Sum	4.360	4.114	9.498
F	0.516	0.131	2.637
Cl	0.032	–	–

UNCORRECTED PROOF

mous reviewers are acknowledged for very useful suggestion and comments leading to the revised and final version of the manuscript which was strongly improved.

Appendix A. Supplementary data

Supplementary data related to this article can be found at http://dx.doi.org/10.1016/j.jsames.2016.08.003.

Table 9
Representative analyses of rosenbuschite [number of ions on the basis of 9 (O,F); S1 = Ti + Zr + Nb + Fe + Mn + Mg; S2=Ca + Na], låvenite [number of ions on the basis of 9(O,F)], eudialyte [number of ions on the basis of 29 (Si,Al,Zr,Ti,Nb)] and catapleiite [number of ions on the basis of 9 O]. Data source: this work, Carbonin et al. (2005) and Table 38 of Comin-Chiaramonti et al. (2005).

Sample	Rosenbuschite		Låvenite		Sample	Eudialyte		Ca-catapleiite	
	RP31	RP33	RP33	RP40		RP33	RP33B	RP33	
SiO_2	31.22	31.37	32.58	30.95	SiO_2	49.98	49.38	SiO_2	44.69
TiO_2	7.63	8.14	3.75	4.37	Al_2O_3	0.10	0.12	ZrO_2	31.00
ZrO_2	14.36	13.42	29.90	27.76	TiO_2	0.40	0.14	CaO	13.82
Nb_2O_5	1.25	1.64	1.40	2.10	ZrO_2	12.46	12.34	Na_2O	0.32
FeO	0.95	0.65	2.97	2.82	Nb_2O_5	1.44	1.85	K_2O	0.01
MnO	2.71	2.95	5.99	6.09	FeO	4.82	5.37	H_2O	9.15
MgO	0.12	0.10	9.10	0.11	MnO	4.20	2.24	Sum	98.99
CaO	24.09	25.39	12.43	12.70	MgO	0.08	0.01		
Na_2O	9.39	9.14	6.80	8.53	CaO	11.85	12.28	Atoms	
F	8.16	8.49-	–	–	Na_2O	11.16	9.02	Si	2.987
Sum	99.87	101.29	101.25	101.20	K_2O	0.26	0.25	Zr	1.008
–O═F	3.43	3.58	2.24	2.43	SrO	0.11	0.02	Ca	0.988
Sum	96.44	97.71	99.01	98.77	La_2O_3	0.40	0.78	Na	0.020
					Ce_2O_3	0.41	1.19	K	0.000
Atoms					Cl	1.16	1.08	Sum	5.003
Si	2.001	1.980	2.131	2.039	–O═Cl	0.26	0.24		
Ti	0.368	0.386	0.185	0.217	Sum	98.59	96.23		
Zr	0.449	0.414	0.954	0.891	Si	25.369	25.371		
Nb	0.036	0.047	0.041	0.063	Al	0.060	0.076		
Fe^{2+}	0.051	0.034	0.163	0.156	Ti	0.154	0.052		
Mn	0.147	0.157	0.332	0.340	Zr	3.085	3.072		
Mg	0.012	0.010	0.009	0.011	Nb	0.331	0.429		
Ca	1.654	1.716	0.871	0.896	Fe^{2+}	2.046	2.317		
Na	1.167	1.120	0.862	1.090	Mn	1.805	0.970		
Sum	5.885	5.863	5.548	5.703	Mg	0.063	0.001		
F	1.654	1.695	1.103	1.201	Ca	6.443	6.757		
S1	1.062	1.048	1.684	1.678	Na	10.981	9.038		
S2	2.822	2.836	1.733	1.986	K	0.168	0.158		
					Sr	0.033	0.001		
					La	0.076	0.185		
					Ce	0.077	0.283		
					Sum	50.693	48.719		
					Cl	1.002	0.943		

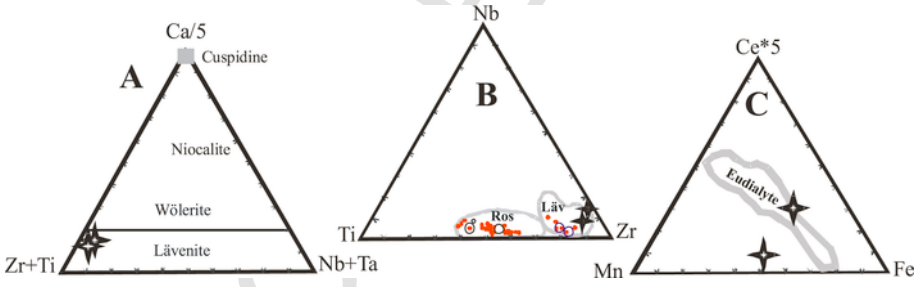

Fig. 10. A: Ca/5-(Nb + Ta)-(Zr + Ti) ternary diagram with data points corresponding to the låvenite analyses of Table 9 (stars) and the main composition of the cuspidine group (grey full square), after Keller and Williams (1995). **B**: Nb—Ti—Zr cation distribution (after Keller and Williams, 1995), for rosenbuschite (Ros) and Låvenite (Låv). Large circles: rosembuschite and låvenite from Table 9; stars, eudialyte. Red dots: compositions from Carbonin et al. (2005). **C**: Fe—Mn—Ce*5 ternary diagram for eudialytes (field of eudialyte from Sjöqvist et al., 2013). (For interpretation of the references to colour in this figure legend, the reader is referred to the web version of this article.)

UNCORRECTED PROOF

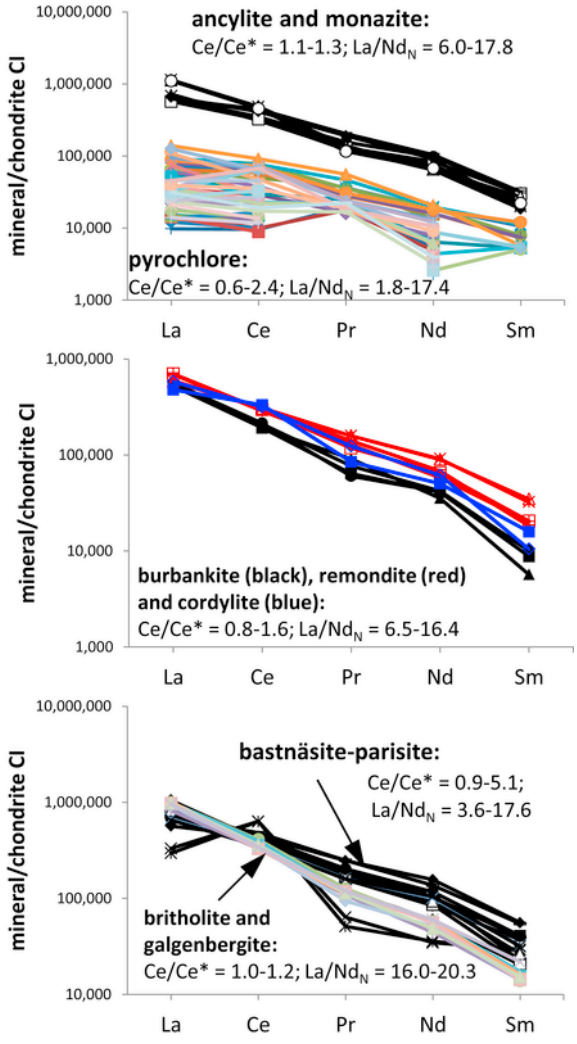

Fig. 11. LREE patterns of REE-bearing minerals normalized to chondrite CI (Barrat et al., 2012); $Ce/Ce^* = Ce/(La \cdot Pr)^{0.5}$, $La/Nd_N = La/Nd$ (both normalized to chondrite CI).

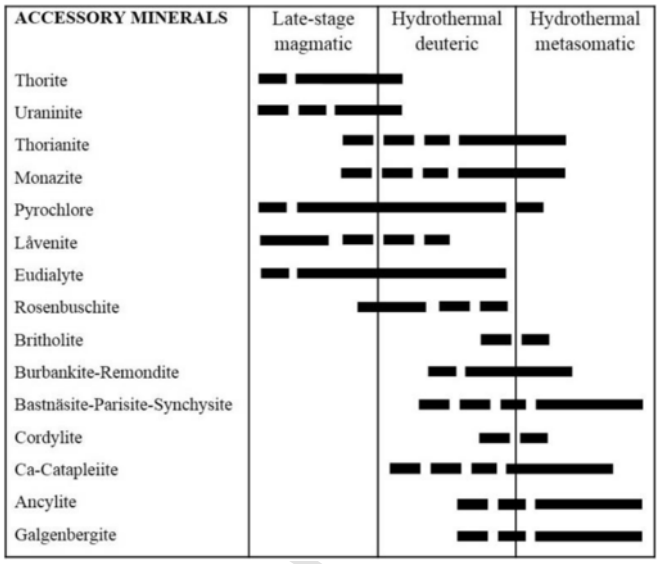

Fig. 12. Bar diagram showing the crystallization history of the accessory minerals in the nepheline syenites and phonolites of Cerro Boggiani agpaitic complex. The diagram roughly attributes each accessory mineral to one or more of the following phases of crystallization: (i) late-stage magmatic, (ii) hydrothermal deuteric (H_2O-rich) and (iii) hydrothermal metasomatic of carbonatitic origin (CO_2-rich). Dashed lines represent low modal content and/or some uncertainty of attribution to the correspondent phase of crystallization.

References

Aksenov, S.M., Rastsvetaeva, R.K., Mitchell, R.H., Chakrabarty, A., 2014. Crystal structure of manganese-rich variety of eudialyte from Suchina hill, India, and manganese ordering in eudialyte group minerals. Crystallogr. Rep. 59, 146–154.

Alaimo, R., Censi, P., 1992. Quantitative determination of major, minor and trace elements on USGS rock standards by inductively coupled plasma mass spectrometry. At. Spectrom. 13, 113–119.

Amaral, G., 1984. Provincia Tapajós e Rio Branco. In: Almeida, F., F:A, Hasui, Y. (Eds.), O Précambriano do Brasil. Edgar Blücher Ltda, São Paulo, pp. 6–35.

Andersen, T., 2014. REE mineral assemblages in igneous rocks: what can be learned from chemographic modelling?. In: Workshop on Accessory Minerals. Universiy of Warsaw, pp. 7–8.

Barrat, J.A., Zanda, B., Moynier, F., Bollinger, C., Liorzou, C., Bayon, G., 2012. Geochemistry of CI chondrites: major and trace elements, and Cu and Zn isotopes. Geochim. Cosmochim. Acta 83, 79–92.

Bastin, G.F., Van Loo, F.J.J., Heijligers, H.J.M., 1984. Evaluation and use of gaussian $\phi(\rho z)$ curves in quantitative electron probe microanalysis: a new optimization. X-Ray Spectrom. 13, 91–97.

Bellezza, M., Merlino, S., Perchiazzi, N., 2003. Chemical and structural study of the Zr, Ti-disilicates in the venanzite from Pian di Celle, Umbria, Italy. In: Geoitalia 2003, 4° Forum Italiano di Scieze della Terra, Bellaria. pp. 604–605.

Belovtiskaya, Y.V., Pekov, I.V., 2004. Genetic mineralogy of burbankite group. New Data Minerals 742 (39), 50–64. UDC 549.

Birkett, T.C., Miller, R.R., Roberts, A.C., Kariano, A.N., 1992. Zirconium bearing minerals of the Srange lake complex, Quebec, Labrador. Can. Mineral. 30, 191–205.

Carbonin, S., Liziero, F., Fuso, C., 2005. Mineral chemistry of accessory minerals in alkaline complexes from the Alto Paraguay province. In: Comin-Chiaramonti, P., Gomes, C.B. (Eds.), Mesozoic to Cenozoic Alkaline Magmatism in the Brazilian Platform. Edusp/Fapesp, São Paulo, pp. 149–158.

Castorina, F., Censi, P., Comin-Chiaramonti, P., Gomes, C.B., Piccirillo, E.M., Alcover Neto, A., Almeida, R.T., Speziale, S., Toledo, M.C., 1997. Geochemistry of carbonatites from eastern Paraguay and genetic relationships with potassicc magmatism: C, O, Sr and Nd isotopes. Mineral. Petrol. 61, 237–260.

Censi, P., Comin-Chiaramonti, P., DeMarchi, G., Longinelli, A., Orué, D., 1989. Geochemistry and C-O isotopes of the Chiriguelo carbonatite (north-eastern Paraguay). J. S. Am. Earth Sci. 3, 295–303.

Cesbron, F., Gilles, C., Pelisson, P., Saugues, J.C., 1988. La remondite-(Ce), un nouveau carbonate de terres rares de la famille de la burbankite. In: Comptes Rendus de l'Académie des Sciences Paris Série II, 307 pp. 915–920.

UNCORRECTED

Chakhmouradian, A.R., Mitchell, R.H., 1998. Lueshite, pyrochlore and monazite-(Ce) from apatite-dolomite carbonatite, Lesnaya Varaka complex, Kola Peninsula, Russia. Mineral. Mag. 62, 769–782.

Clavier, N., Podor, R., Dacheux, N., 2011. Crystal chemistry of the monazite structure. J. Eur. Ceram. Soc. 31, 941–976.

Comin-Chiaramonti, P., De Min, A., Girardi, V.A.V., Gomes, C.B., 2014. Carbonatites and primary carbonates in the Rio Apa and Amambay regions, NE. Parag. Lithos 188, 84–96.

Comin-Chiaramonti, P., Gomes, C.B., Censi, P., Gasparon, M., Velázquez, V.F., 2005. Alkaline complexes from the Alto Paraguay province at the border of Brazil (Mato Grosso do Sul state) and Paraguay. In: Comin-Chiaramonti, P., Gomes, C.B. (Eds.), Mesozoic to Cenozoic Alkaline magmatism in the Brazilian Platform. Edusp/Fapesp, São Paulo, pp. 71–148.

Comin-Chiaramonti, P., Gomes, C.B., De Min, A., Ernesto, M., Gasparon, M., 2015. Magmatism along the high Paraguay River at the border of Brazil and Paraguay: a review and new constraints on emplacement ages. J. S. Am. Earth Sci. 58, 72–81.

Dal Negro, A., Rossi, G., Tazzoli, V., 1975. The crystal structure of ancyllite, $(REE)_x(Ca,Sr)_{2-x}(CO_3)_2(OH)_x(2-x)H_2O$. Am. Mineral. 60, 280–284.

Deer, W.A., Howie, R.A., Zussman, J., 1997. Disilicates and ringsilicates Rock-forming Minerals. vol. 1B. The Geological Society of London, 333.

De La Roche, H., Leterrier, P., Grandclaude, P., Marchal, M., 1980. A classification of volcanic and plutonic rocks using $R_1.R_2$ diagram and major-element analyses. Its relationships with current nomenclature. Chem. Geol. 29, 183–210.

Drake, M.J., Weill, D.F., 1972. New rare element standeards for electron microprobe analysis. Chem. Geol. 10, 179–181.

Enrich, G.E.R., Ruberti, E., 2004. Química mineral de britholitas em nefelina microsienitos da suíte alcalina da Ilha Monte de Trigo (SP). In: XLII Congresso Brasileiro de Geologia, Araxá, 2004.

Enrich, G.E.R., Gomes, C.B., Ruberti, E., 2010. Química mineral de carbonatos de elementos terras raras em nefelina sienitos e fonólitos agpaíticos do maciço de Cerro Boggiani, Província Alto Paraguay, Paraguai. In: X Congresso de Geoquímica dos Países de Língua Portuguesa, Porto, 2010, Actas. pp. 223–227.

Enrich, G.E.R., Gomes, C.B., Ruberti, E., Azzone, R.G., 2011. Silicatos de zircônio do grupo da cuspidina-wöhlerita nas rochas vulcânicas agpaíticas do maciço alcalino de Cerro Boggiani, Paraguai. In: V Simpósio de Vulcanismo e Ambientes Associados, Cidade de Goiás, Anais, CD-ROM.

Enrich, G.E.R., Gomes, C.B., Ruberti, E., Azzone, R.G., 2012. Eudialitas do maciço alcalino de Cerro Boggiani, Paraguai: ocorrência e composição química. In: 46° Congresso Brasileiro de Geologia, Santos, CD-ROM.

Förster, H.-J., 1999. The chemical composition of uraninite in Variscan granites of Erzgebirge, Germany. Mineral. Mag. 63, 239–252.

Gieré, R., 1996. Formation of rare earth minerals in hydrothermal systems. The Mineralogical Society Series 7. In: Jones, A.P., Wall, F., Williams, C.T. (Eds.), Rare Earth Minerals: Chemistry, Origin and Ore Deposits, Chapman & Hall, London, pp. 105–150.

Giester, G., Ni, Y., Jarosch, D., Hughes, J.M., Rønsbo, J., Yang, Z., Zemann, J., 1998. Cordylite-(Ce): a crystal chemical investigation of material from four localities, including type material. Am. Mineral. 83, 178–184.

Gomes, C.B., Laurenzi, M.A., Censi, P., De Min, A., Velázquez, V.F., Comin-Chiaramonti, P., 1996. Alkaline magmatism from northern Paraguay (Alto Paraguay): a Permo-Triassic province. In: Comin-Chiaramonti, P., Gomes, C.B. (Eds.), Alkaline magmatism in Central-Eastern Paraguay. Relationships with Coeval Magmatism in Brazil. Edusp/Fapesp, São Paulo, pp. 223–230.

Haas, J.R., Shock, E.L., Sassani, D.C., 1995. Rare earth elements in hydrothermal system: estimates of standard partial molar thermodynamic properties of aqueous complexes of the rare earth elements at high pressures and temperatures. Geochim. Cosmochim. Acta 59, 4329–4350.

Harlov, D.E., Hetherington, C.J., 2010. Partial high-grade alteration of monazite using alkali-bearing fluids: experiment and nature. Am. Mineral. 95, 1105–1108.

Hogarth, D.D., 1989. Pyrochlore, apatite and amphibole: distinctive minerals in carbonatite. In: Bell, K. (Ed.), Carbonatites: Genesis and Evolution. Chapman and Hall, London, U.K, pp. 105–148.

Hogarth, D.D., Rushforth, P., McKorkell, R.H., 1988. The Blackburn carbonatites, near Ottawa, Ontario: dikes with fluidized emplacement. Can. Mineral. 26, 377–390.

Hogarth, D.D., Horne, J.E.T., 1989. Non-metamict uranoan pyrochlore and uranpyrochlore from tuff near Ndale, Fort Portal area, Uganda. Mineral. Mag. 53, 257–262.

Hornig-Kjarsgaard, I., 1998. Rare earth elements in sövitic carbonatites and their mineral phases. J. Petrol. 39 (11–12), 2105–2121.

Jarosevich, E.N., 2002. Electron microprobe standards, mineral standards, microbeam standards. Smithson. Microbeam Stand. J. Res. Natl. Inst. Stand. Technol. 107, 681–685.

Johnsen, O., Grice, G.D., 1999. The crystal chemistry of the eudyalite group. Can. Mineral. 37, 865–891.

Karup-Møller, S., Hansen, J.R., Sørensen, S., 2010. Eudialyte decomposition minerals with new hitherto undercribed phases from the Ilimaussaq complex, south Greenland. Bull. Geol. Soc. Den. 58, 75–88.

Keller, J., Williams, T.C., 1995. Niocalite and wöhlerite from alkaline and carbonatite rocks at Kaisertuhl, Germany. Mineral. Mag. 59, 561–566.

Khomyakov, A.P., 1995. Mineralogy of Hyperagpaitic Alkaline Rocks. Oxford Science Publications, 222.

Kogarko, L.N., 1987. Alkaline rocks of the eastern part of the Baltic shield (Kola peninsula). In: Fitton, J.G., Upton, B.G.J. (Eds.), Alkaline Igneous Rocks. Geological Society of London, Special Publication, 30. pp. 531–544.

Kogarko, L.N., Burnham, C., Shettle, D., 1977. Water regime in alkalic magmas. Geochem. Int. 14, 1–8.

Kogarko, L.N., Ryabchikov, I.D., Sørensen, H., 1974. Liquid fractionation. In: Sørensen, H. (Ed.), The Alkaline Rocks. John Wiley, London, pp. 488–500.

Le Maitre, R.W., 1989. A Classification of Igneous Rocks and Glossary of Terms. Blackwell Science Publication, Oxford, 193.

Lemarão, C.N., Dall'Agnol, R., Lafon, J.-M., Lima, E.F., 2002. Geology, geochemistry and Pb-Pb zircon geochronology of the paleoproterozoic magmatism of Vila Riozinho, Tapajos province, Amazonian Craton, Brazil. Precambr. Res. 119, 189–223.

Lumpkin, G.R., Ewing, R.C., 1995. Geochemical alteration of pyrochlore group minerals; pyrochlore subgroup. Am. Mineral. 80, 732–743.

Mahato, A.C., Ren, M., Chakrabarti, A., Sen, A.K., Rajesh, H.M., Shindo, K., 2013. Reconstruction of magmatic to deuteric stages of the eudyalite-bearing Sushina syenite gneiss, western Bengala, India. J. Ind. Geol. Congr. 5, 77–93.

Mellini, M., 1981. Refinement of the crystal structure of låvenite. Tschermaks Mineral. Petrogr. Mittl. 28, 99–112.

Merlino, S., Pasero, S., Bellezza, M., Pushcharovsky, D.Y., Gobecchia, E.R., Zubkova, N.V., Pehov, I.V., 2004. Crystal structure of calcium catapleite. Can. Mineral. 42, 1037–1045.

Mills, S.J., Kartashov, P., Kampf, A.R., Konev, A.A., Koneva, A.A., Raudsepp, M., 2012. Cordylite, a new mineral from the Biraya Fe-REE deposit, Irkutsk, Russia. Can. Mineral. 50, 1281–1290.

Mitchell, R.H., 2015. Primary and secondary niobium mineral deposits associated with carbonatites. Ore Geol. Rev. 64, 626–641.

Moine, B., Ramambazafy, A., Rakotondrazafy, M., Ravolomiandrinarivo, B., Cuney, M., Parseval, P., 1998. The role of fluor-rich fluids in the formation of the thorianite and sapphire deposits from SE Madagascar. In: Goldschmidt Conference, Toulouse. pp. 999–1000.

Niet, Y., Hughes, J.M., Mariano, A.N., 1995. Crystal chemistry of monazite and xenotime structures. Am. Mineral. 80, 21–26.

Oberti, R., Ottolini, L., Della Ventura, G., Parodi, G.C., 2001. On the symmetry and crystal chemistry of britholite: new structural and microanaytical data. Am. Mineral. 86, 1066–1075.

Pekov, I.V., Chukanov, N.V., Kononkova, N.N., Zadov, A.E., Belovitskaya, Y.V., 2000. Remondite-(La), $Na_3(La,Ce,Ca)_3(CO_3)_5$ – a new mineral of the burbankite family from the Khibina Massif, Kola peninsula. Zap. Vserossiyskogo Mineral. Obshchestva 129 (1), 53–60 (in Russian).

Pekov, I.V., Pasero, M., Yaskovskaya, A.N., Chukanov, N.V., Yu Puschcharovsky, D., Merlino, S., Zubkova, N.V., Kononkova, N.N., Men'shikov, Y.P., Zadov, A.E., 2007. Fluorbritholite, $(Ca, REE)_5[(Si,P)O_4]_3F$, a new mineral: description and crystal chemistry. Eur. J. Mineral. 19, 95–102.

Pekov, I.V., Petersen, O.V., Voloshin, A.V., 1997. Calcio-ancylite-(Ce) from Ilimaussaq and Narssarssuk, Greenland, Kola peninsula and Polar Urals, Russia; ancylite-(Ce)-calcioAncylite-(Ce) an isomorphous series. Neues Jahrb. Mineral. Abh. 171, 309–322.

Putzer, H., Van den Bomm, G., 1962. Über einige Vorkommen von Alkaligesteinen in Paraguay. Geol. Jahrb. 79, 423–443.

Ridolfi, F., Renzulli, A., Santi, P., Upton, B.G.J., 2003. Evolutionary stages of crystallization of weakly peralkaline syenites: evidence from ejecta in the plinian deposits of Agua de Pau volcano (São Miguel, Azores Islands). Mineral. Mag. 67, 749–767.

Ridolfi, F., Renzulli, A., Macdonald, R., Upton, B.G.J., 2006. Peralkaline syenite autoliths from Kilombe volcano, Kenya Rift valley: evidence for subvolcanic interaction with carbonatitic fluids. Lithos 91, 373–392.

Roeder, P.L., 1985. Electron-microprobe analysis of minerals for rare earth elements: use of calculate peak-overlap corrections. Can. Mineral. 23, 263–271.

Ruberti, E., Enrich, G.E.R., Gomes, C.B., Comin-Chiaramonti, P., 2008. Hydrothermal REE fluorcarbonate mineralization at Barra do Itapirapuã, a multiple stockwork carbonatite, southern Brazil. Can. Mineral. 46, 1361–1374.

Sjöqvist, A.S.L., Cornell, David H., Andersen, T., Erambert, M., Ek, M., Leijd, M., 2013. Three compositional varieties of rare-earth element ore: eudialyte-group minerals from the Norra Kårr alkaline complex, southern Sweden. Minerals 3, 94–120.

Smith, M.P., Henderson, P., Campbell, L.S., 2000. Fractionation of the REE during hydrothermal processes: constraints from the Bayan Obo Fe–REE–Nb deposit, Inner Mongolia, China. Geochim. Cosmochim. Acta 64, 3141–3160.

UNCORRECTED PROOF

Soares, J.E., Berrocal, J.U., Fuck, R.A., Mooney, W.D., Ventura, D.B.R., 2006. Seismic characteristics of central Brazil crust and upper mantle; a deep seismic refraction study. J. Geophys. Res. 111 (B12302), 1–31.

Sørensen, H., 1997. The agpaitic rocks, an overview. Mineral. Mag. 61, 485–498.

Speziale, S., Censi, P., Comin-Chiaramonti, P., Ruberti, E., Gomes, C.B., 1997. Oxygen and carbon isotopes in the Barra do Itapirapuá and Mato Preto carbonatites (southern Brazil). Mineral. Petrogr. Acta 40, 137–157.

Stoppa, F., Schiazza, M., 2014. Extreme chemical conditions of crystallisations of Umbrian Melilitolites and wealth of rare, late stage/hydrothermal minerals. Central Eur. J. Geosci. 6 (4), 549–564.

Sun, S.S., McDonough, W.F., 1989. Chemical and isotopic systematics of oceanic basalts. In: Saunders, D., Norry, M.J. (Eds.), Magmatism in the Ocean Basins. Geological Society Special Publication, 42. pp. 313–345.

Toledo, M.C.M., Pereira, V.P., 2003. Ocorência e variabilitade da comosição dos fosfatos do grupo da monazita em carbonatitos. Pesqui. Geociênc. 30, 83–95.

Torro, L., Villanova, C., Castillo, M., Campeny, M., Gonçalves, A.O., Melgarejo, J.C., 2012. Niobium and rare earth minerals from the Virilundo carbonatite, Namibia. Mineral. Mag. 76, 393–409.

Wagner, C., Mokhtari, A., Deloule, E., Chabaux, F., 2003. Carbonatite and alkaline magmatism in Taouririt (Morocco): petrological, geochemical and Sr–Nd isotope characteristics. J. Petrol. 44 (5), 937–965.

Walter, F., Bojar, H.-P., Hollerer, C.E., Mereiter, K., 2013. The crystal structure of galgenbergite-(Ce), $CaCe_2(CO_3)_4 \bullet H_2O$. Mineral. Petrol. 107, 189–199.

Williams, M.L., Jercinovic, M.J., Hetherington, C.J., 2007. Microprobe monazite geochronology: understanding geological processes by integrating compositions and geochronology. Annu. Rev. Earth Planet. Sci. 35, 137–175.

Woolley, A.R., Platt, R.G., 1988. The peralkaline nepheline syenite of the Junguni intrusion, Chilwa province, Malawi. Mineral. Mag. 52, 425–433.

Zaitsev, A.N., Wall, F., LeBas, M.J., 1998. REE-Sr-Ba minerals from the Khibina carbonatites, Kola Peninsula, Russia: their mineralogy, paragenesis and evolution. Mineral. Mag. 62, 225–250.

Zurevinski, S.E., Mitchell, R.H., 2004. Extreme compositional variation of pyrochlore-group minerals at the Oka carbonatite complex, Quebec: evidence of magma mixing?. Can. Mineral. 42, 1159–1168.

UNCORRECTED PROOF